Uncl. Portions

011764-1-F

(incl. Appendix)

11764-1-F = RL-2222

I

INTRODUCTION

(U) This final report culminates a 21-month investigation spanning two Contracts (F33615-72-C-1439, F33615-73-C-1174) on methods of reducing non-specular scattering. The major tools used in accomplishing this objective were computer programs that numerically solve the integral equations governing the surface fields on two-dimensional structures, but laboratory experiments were also carried out for the purpose of verifying the programs. Much of the experimental work in the present (second) Contract was performed by AFAL personnel at WPAFB, who generously supplied the data appearing in this and other reports issued during the study.

(U) The computer programs determine the surface fields at discrete sampling points distributed over the profiles of cylindrical bodies, then calculate the scattered field from the surface field distribution. If the surface sampling were fine enough, and if a laboratory experiment were to be carefully and accurately carried out, the results of the computations and the measurements would be indistinguishable. Thus, although the investigation focussed on the use of the programs and the interpretation of the results, the conclusions drawn are largely based on "experimental" data. That the data were produced digitally is of no real consequence, and the reader will perceive that we occasionally refer to computed results as "digital", or "numerical" experiments, or simply "experiments".

(U) Non-specular scattering is quite literally any that is not specular and is produced by electrical or geometrical discontinuities, or by discontinuities in the illumination of the surface. Edges and shadow boundaries are examples of each kind. The surfaces of non-specular scattering can be resolved into two classes, one due to surface waves and the other due to direct diffraction from discontinuities such as edges. Surface waves include creeping and traveling waves, and one is distinguished from the other according to the surface illumination: traveling waves build up over lit surfaces while creeping waves decay along shaded surfaces. Edge

1

MISSING
PAGE

MISSING
PAGE

MISSING
PAGE

CHAPTER II
ELECTRIC RESISTIVE SHEETS

2.1 Introduction

(U) The non-specular backscattering from thin metallic structures, such as the fins of a missile or the wings of an aircraft, is dominated by the returns from the edges, and the aspect angles over which this scattering is significant typically range out to 40 or 50 degrees from edge-on incidence. Both the leading and the trailing edges participate for arbitrary incident polarization, but for analytical purposes it is convenient to address the specific cases of E- or H-polarization, for which the incident electric or magnetic vector, respectively, is parallel to an edge. The problem of reducing the non-specular return then becomes the dual task of reducing it separately for both polarizations. If the reduction can be accomplished for each polarization, and if the technique required for each does not degrade the performance for the other, the treatments will be effective for any polarization.

(U) At precisely edge-on incidence the trailing edge contribution is negligible because, for a profile of non-zero thickness, the trailing edge is shadowed. As the aspect angle swings away from edge-on, eventually exposing the trailing edge to the incident wave, the H-polarized return builds up rapidly due to a travelling wave reflection at the rear, and this happens to be the dominant source of non-specular scattering for H-polarized incidence. There is also a small, but non-zero, contribution due to the leading edge. By contrast, the trailing edge return for E-polarization remains small in comparison to that from the leading edge, and the leading edge contribution increases quite slowly as the aspect angle swings from edge-on out to 50 degrees or so. The magnitude of the travelling wave return for H-polarization is comparable to that of the leading edge return for E-polarization.

(U) By the use of a two-dimensional impedance boundary condition computer program (RAM1B) developed in the predecessor Contract we found that the travelling wave returns were relatively easy to reduce with appropriate surface coatings, hence we turned to the more difficult task of reducing the leading edge

MISSING
PAGE

MISSING
PAGE

(U) The analogy between the resistive sheet and waveguide loads extends even to the physical length required to achieve a "good" match. Experience has shown that high performance broadband loads must be gently tapered lest new sources of reflection be generated, and the same result prevails in the use of resistive sheets: the wider the sheet, the more effective it is. In a practical application, however, there is a limitation on permissible sheet width and the problem of extracting optimum performance becomes one of finding the most favorable rate of resistance taper. Our studies have shown that a quadratic rate of change is optimum, as will become apparent.[*]

(U) A total of five kinds of distributions have been examined during the contract and their relative rates of build-up are sketched in Fig. 2-1. The generic forms of the distributions are

$$R(s) = R_{max} (s/\ell)^n \, , \tag{2.1}$$

$$R(s) = R_a + R_b e^{-ms/\ell} \, , \tag{2.2}$$

where $R(s)$ is the resistance normalized to 377 ohms at any point along the sheet located by the distance s, and ℓ is the total sheet width. The variations represented by (2.1) and (2.2) are valid for curved sheets as well as flat ones, since s is a distance measured along the surface of the sheet from one edge. Equation (2.1) is a power distribution while (2.2) is exponential and the constants R_{max}, R_a and R_b must be specified either in ohms or normalized with respect to 377 ohms, depending on which version of the computer program is used. The exponent n need not be an integer, but thus far none other than integral values have been used; the exponential form (2.2) has been used only for the purpose of synthesizing discontinuities in the slope of the resistance variation as controlled by the parameter m.

---

[*] (U) Early in the predecessor contract we dealt with linear and square law distributions. Later, as higher order variations such as the cubic were investigated, we felt it appropriate to replace the term "square law" with "parabolic". Now it is algebraically more descriptive to use the term "quadratic" instead of "parabolic" or "square law".
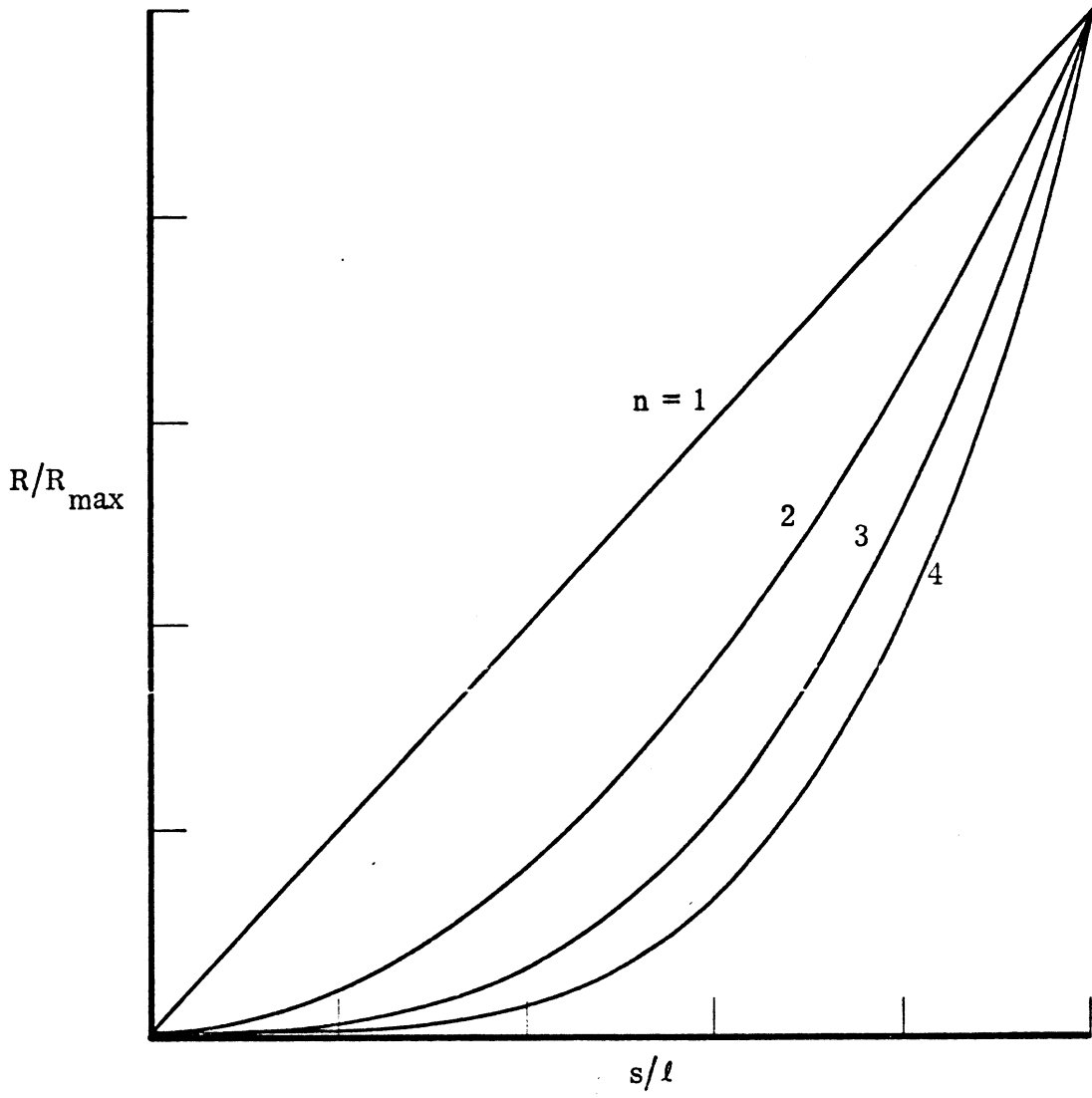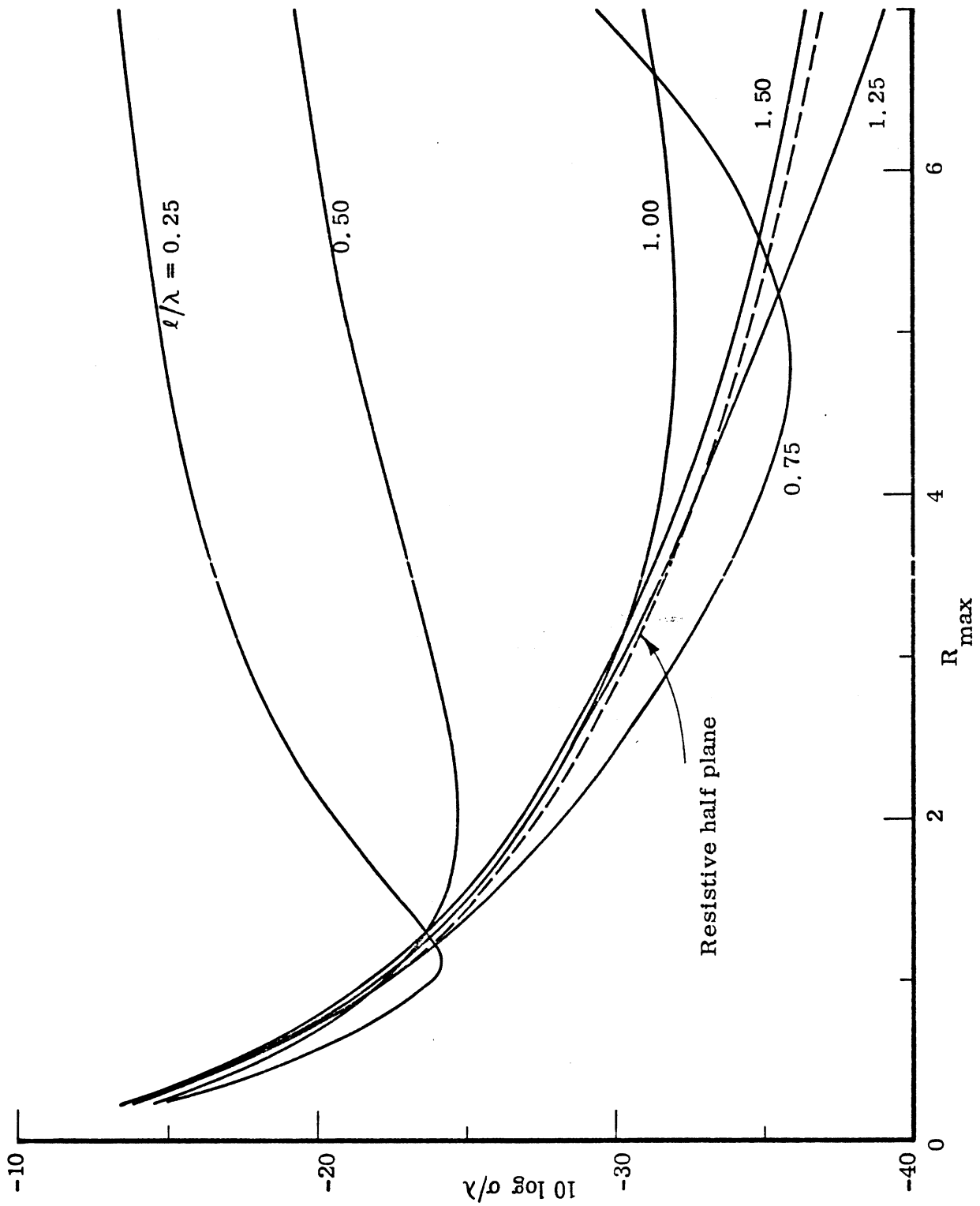
(U) FIG. 2-1: Examples of resistance distributions for linear, quadratic, cubic and quartic laws.
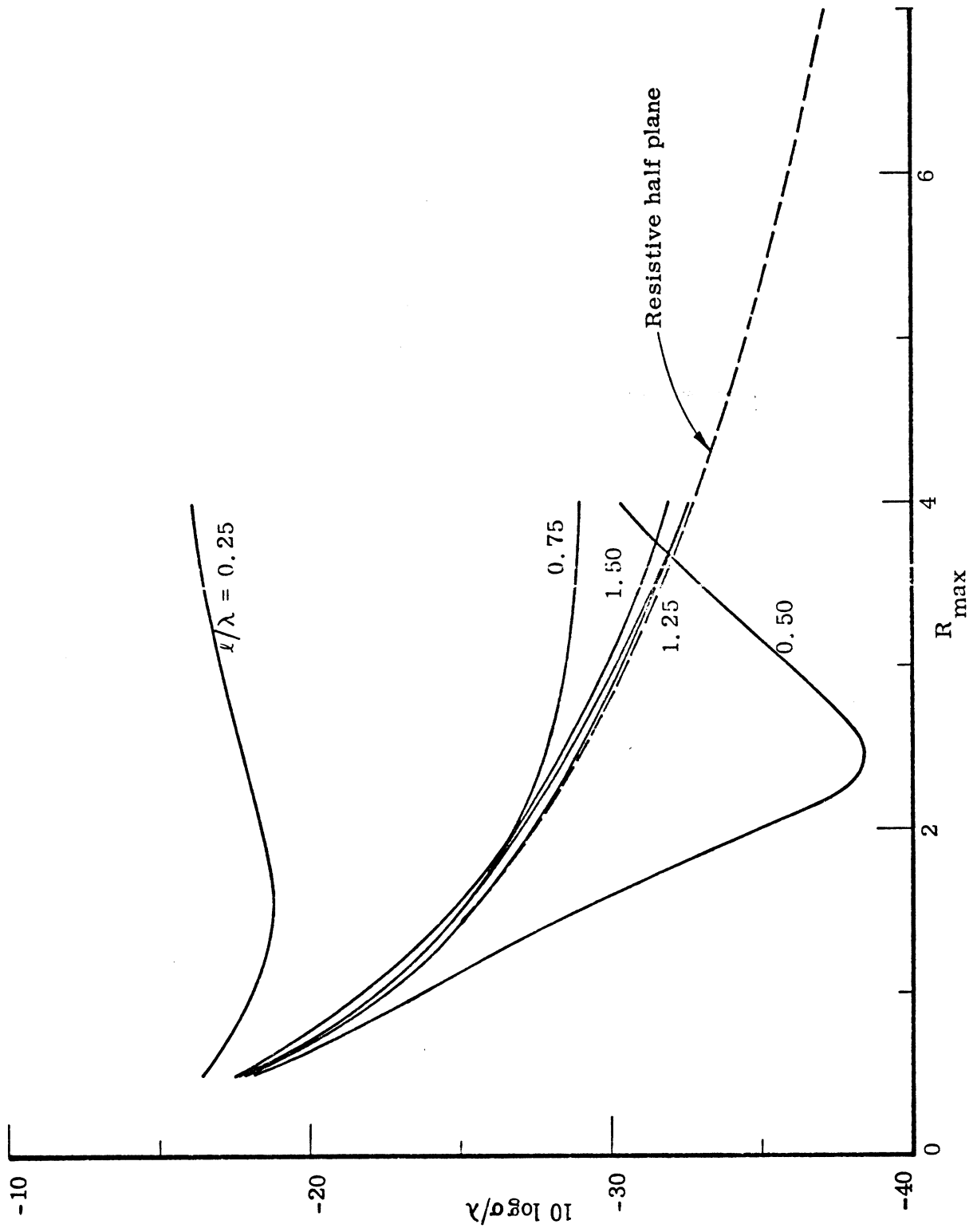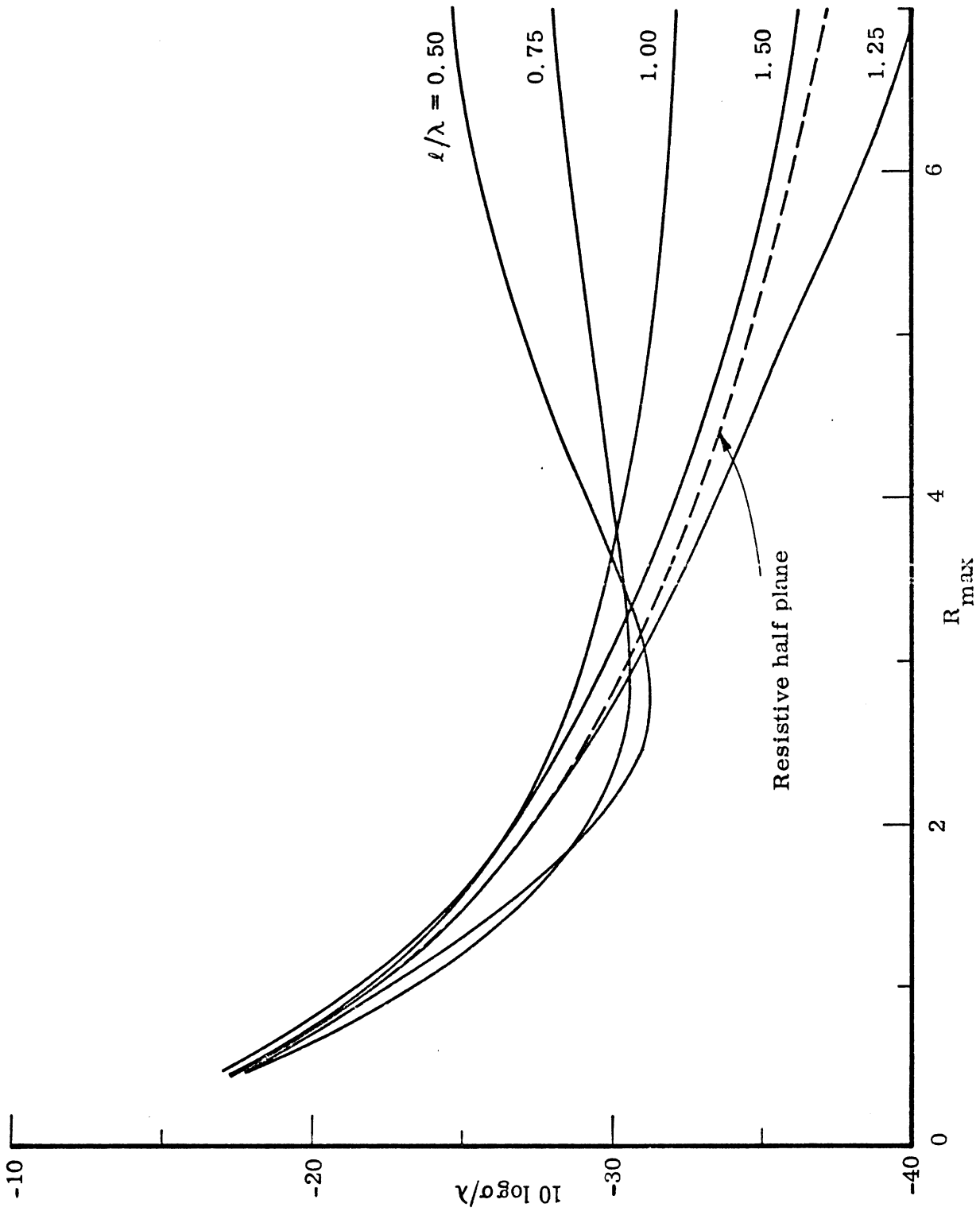
MISSING
PAGE

MISSING
PAGE
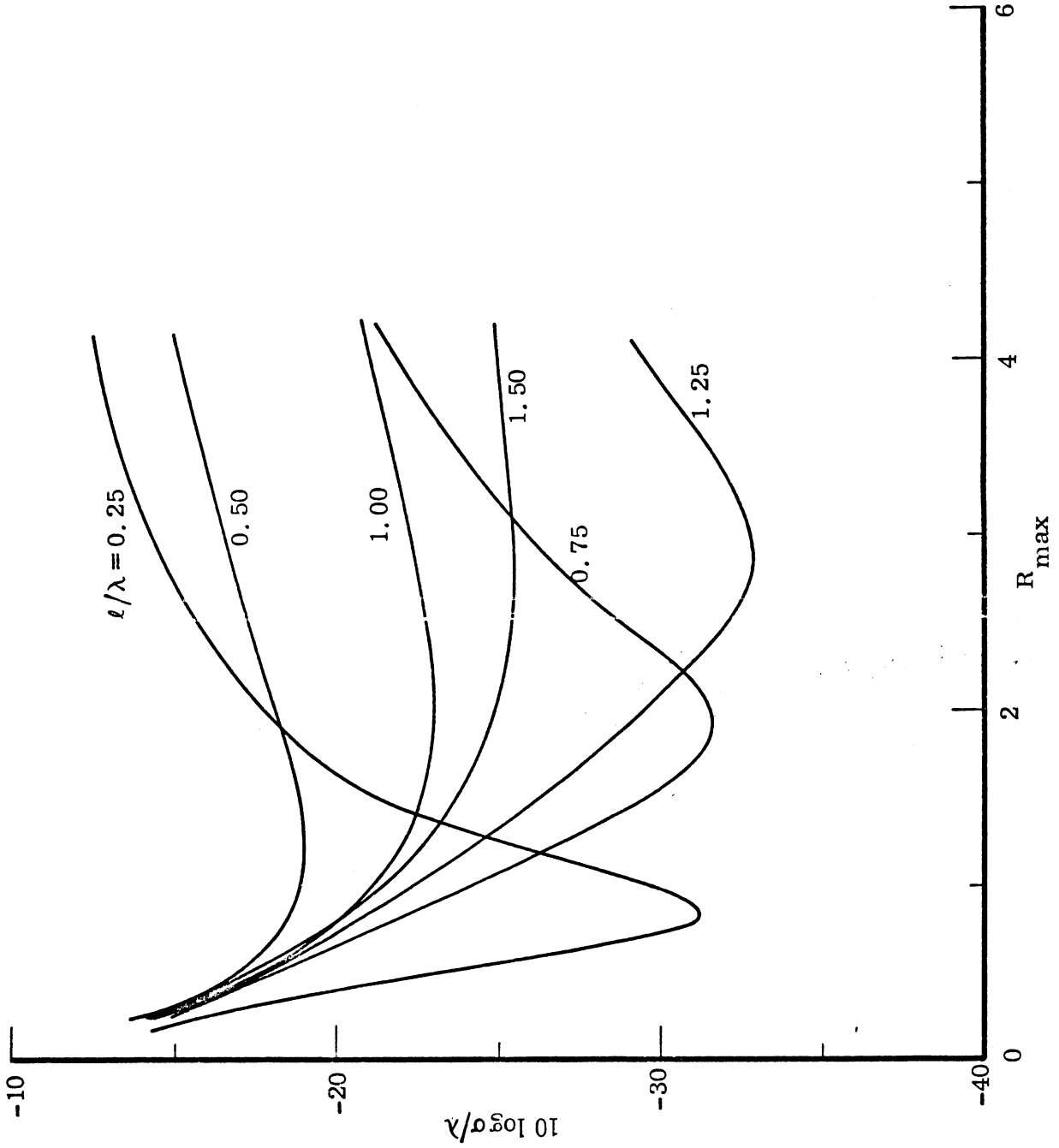
(U) FIG. 2-3: Edge-on scattering from cylinder-sheet combination for linear resistance distribution.

(U) FIG. 2-4: Edge-on scattering from cylinder-sheet combination for quadratic resistance distribution.
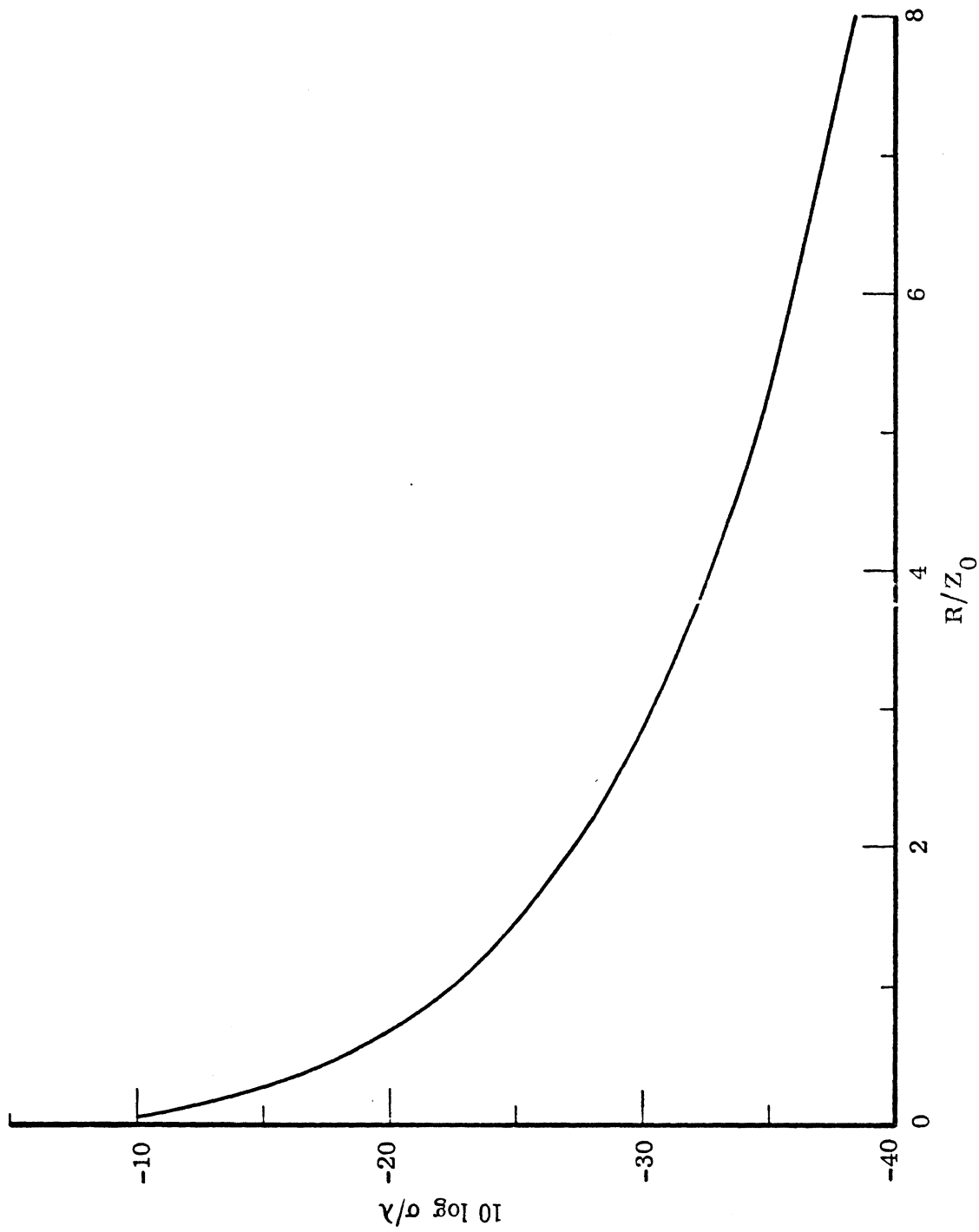
13

(U) FIG. 2-5: Edge-on scattering from cylinder-sheet combination for cubic resistance distribution.

(U) FIG. 2-6: Edge-on scattering from cylinder-sheet combination for quartic resistance distribution.

MISSING
PAGE

(U) FIG. 2-7: Edge–on cross section of resistive half–plane of resistance R.

reference. It can be seen that the theoretical curve is a quite good approximation of the total return, at least for the smaller values of R_{max} and/or the wider sheets. We surmised that, by virtue of the close agreement for these cases, the leading edge of the sheet is the dominant source of scattering and that the theoretical values represented by Fig. 2-7 were probably quite accurate.

(U) A model of the net scattering by the sheet-treated ogival cylinder was subsequently assumed to consist of only two sources: the leading and trailing edges of the sheet. For arbitrary angles of incidence a third contribution would have to be included due to the trailing edge of the metallic cylinder, but at edge-on incidence this source is totally negligible. The trailing edge of the sheet joins the leading edge of the cylinder and while it could be argued that each makes a contribution, it is not possible to separate one from the other since they occupy the same point in space. Thus, although in the analysis below we speak of the "trailing edge" component of the resistive sheet, it actually refers to a junction effect, and the value deduced for the "trailing edge" return depends quite strongly on the nature of the body or edge to which the sheet is attached.

(U) Thus the conceptual model of the scattering of the sheet-cylinder ensemble is the sum of a pair of returns, P_{ℓ} and P_t, due to the leading and trailing edges of the sheet. If the origin is fixed at the leading edge, the total two-dimensional scattering is then

$$P = P_{\ell} + P_t e^{i2k\ell} , \qquad (2.3)$$

where ℓ is the distance between the two edges (i.e., the sheet width) and the phase factor serves to account for two-way delay in the return from the rear edge. Since the theoretical values listed in Appendix A are normalized to that of a metallic half plane, it is convenient to write

$$P_c = A + B e^{i2k\ell} , \qquad (2.4)$$

where $P_c = P/P_0$, $A = P_{\ell}/P_0$, $B = P_t/P_0$ and $P_0 = -i/2$. The left side of

18

(2.4) is directly obtainable from the output of program RISK (when the sign error is accounted for) and is, of course, a complex number. Since A is presumably known for every R_{max}, we can solve (2.4) for the normalized trailing edge component B. The deduced values are plotted for the linear case in Fig. 2-8 and it is quickly seen that the trailing edge can be a stronger scatterer than the leading edge. Moreover, although the data are not shown, the phase of B is essentially independent of the leading edge resistance as well as the sheet width.

(U) Figure 2-8 displays a distinct pattern of increasing trailing edge contribution with decreasing sheet width for fixed R_{max}, suggesting that it is the discontinuity in the slope of the resistance distribution at the rear edge that produces the scattering. When the data are replotted as in Fig. 2-9 as a function of R_{max}/ℓ (instead of R_{max}) it is apparent that, aside from dispersions in the display, the trailing edge contribution is given approximately by

$$|B| = 0.048 R_{max}/\ell .$$

Thus the trailing edge scattering is directly proportional to the slope of the resistance curve there.

(U) By way of verifying this concept, we carried out another numerical experiment using an exponential variation of the form

$$R = R_{max} e^{-mx/\ell}$$

where s is the distance rearward from the leading edge. The sheet width was fixed at 1λ and the slope of the resistance curve depends upon both R_{max} and the constant m in the exponent. Nine discrete values for m were chosen, ranging from about 0.1 to 0.9. Using the same procedures outlined above, the amplitude of the trailing edge contribution was extracted and the results are plotted in Fig. 2-10 as a function of the slope at the rear edge. The deduced value of the dependence on slope is

$$|B| = 0.045 \tan \delta ,$$

MISSING
PAGE

MISSING
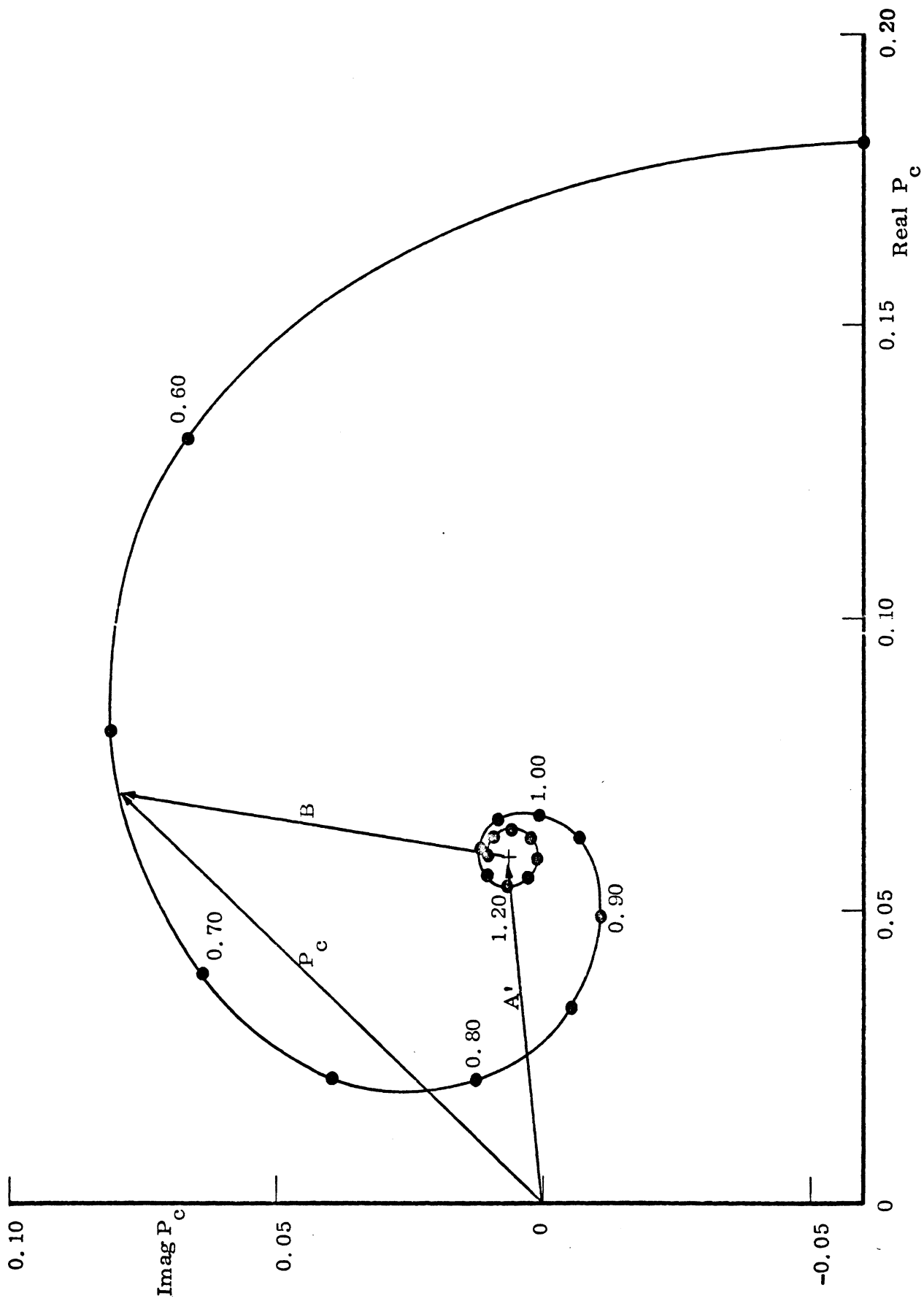## PAGE

MISSING
PAGE

MISSING
PAGE

MISSING
PAGE

MISSING
PAGE

MISSING
PAGE

MISSING

PAGE

where, for this case, A' = 0.0600 (which is slightly greater than the theoretical value), n = 1.282 and B is the complex trailing edge component, which is essentially a small constant for $l \geq \lambda$ and a rapidly changing function of l for $l < \lambda$. Equation (2.6) differs conceptually from the previous model postulated [equation (2.4)] only in the presence of the factor n in the exponent of the phase term. Calculating B from (2.5) was straightforward, but the results were dismal disappointments, both with A' and n as specified above as well as for other values. Invariably oscillatory values for $|B|$ were obtained for $l \geq \lambda$, and instead of a constant value of about 0.0055, as inferred from the undulations in the patterns, $|B|$ inevitably traced out a sinusoidal curve with increasing l, rising to peaks as large as 0.01 and attaining nulls as low as 0.0015. Evidently there was a flaw in the postulated model.

(U) In order to resolve the difficulty, we plotted P_c on the complex plane and the result is the spiral shown in Fig. 2-14. Any point on the spiral is the phasor sum of the leading and trailing edge returns and since the phase reference has been fixed at the leading edge, A' remains constant. As the sheet becomes progressively wider, the trailing edge return B rotates counterclockwise and diminishes in amplitude at the same time. The diagram makes it clear that the only flaw in the model was that A' had been assumed purely real when in fact it has a small but influential reactive component. This small reactive component suggests that the effective center of the scattering from the edge actually lies a small fraction of a wavelength inward from the edge itself. It corroborates the theoretical prediction (found near the end of Section A.4 of Appendix A) of precisely such an effect. A few exploratory calculations showed that the optimum values of A' and n are A' = 0.059+i0.00641, n = 1.290. Using these values, equation (2.5) was solved for B for all the lengths used to construct Fig. 2-13, and the result is plotted in Fig. 2-15.

(U) The mean variation in $|B|$ has been indicated by a smooth solid line, but careful examination of the figure shows that the datum points may lie slightly off the smooth curve. The amplitude $|A'|$ has been indicated as a dashed line running horizontally across the graph, since A' was assumed to be independent of l.

(U) FIG. 2-14: A plot of P_c on the complex plane.

MISSING
PAGE

Note that although the two intersect near $l = 0.70\lambda$, the null in Fig. 2-13 occurs near $l = 0.80\lambda$ because the relative phase between them is not 180°. The decay of B appears to be exponential and bottoms out at a threshold value of $|B| \simeq 0.005$, and seems to have no inclination to fall below this level. We feel the threshold level is related to the geometrical nature of the junction between the sheet and the body and is thus a lower limit that cannot be further lowered without a modification of the metallic body itself.

(U)The above analysis strengthened the conceptual model that the sources of scattering are concentrated near the leading and trailing edges of the resistive sheet. It shows that an unvarying leading edge component pegged at very nearly the theoretical resistive half plane value is almost correct, but that it must be allowed to take on a slightly reactive character. And although the parameters A' and n had been determined for this particular case of a quadratic distribution for $R_{max} = 4.0$, it was obviously of interest to determine the corresponding values for other R_{max} and resistive distributions.

2.5 Other Cases

(U)A full scale analysis of all the cases examined thus far would have been prohibitively costly, hence we settled for a detailed examination of only three additional cases: a quadratic distribution having $R_{max} = 10.0$ (instead of 4.0), and linear and cubic distributions having $R_{max} = 4.0$. The first would show the effect of increasing R_{max} and the remaining two would allow us to compare the effects of three different distributions, all rising to the same leading edge resistance. In addition, it would be of interest to see how the threshold value discovered in Fig. 2-15 would depend upon other distributions and other values of R_{max}. Unfortunately, as will be shown in a moment, the sheets used in the three additional data sets never grew wide enough to reveal the threshold levels and our curiosity remains unsatisfied.

(U) Figure 2-16 displays the edge-on cross sections of these test cases, and it will be perceived that the amplitude data from Fig. 2-13 have been transferred to and included in this figure. Note that the linear distribution is the least effective of the four and that the quadratic variation for $R_{max} = 10.0$ is not as effective as

31

MISSING
PAGE

one for which R_{max} = 4.0, at least for sheets less than 1.2λ wide. The cubic distribution yields better performance than either of the parabolic ones for some sheet widths, but poorer performance for others.

(U)Figures 2-17 through 2-19 display the spirals for the linear, quadratic (R_{max} = 10.0) and cubic distributions. Note that the decay rate for the linear case (Fig. 2-17) is much smaller than for the others, as might have been inferred from Fig. 2-16, and that the cubic spiral undergoes a decided change in decay rate at a sheet width of 1λ. The reason for this abrupt change has not been isolated, but its effect influences the deduced behavior of the trailing edge component. The leading edge component A' was determined graphically from magnified versions of Figs. 2-17 through 2-19 and are summarized in Table 2-1. Note that the deduced

(U)Table 2-1: Deduced Leading Edge Components

| Distribution	R_{max}	Real (A')	Imag (A')
linear	4.0	.0586	.00680
quadratic	4.0	.0590	.00641
cubic	4.0	.0582	.00900
quadratic	10.0	.0242	.00316

values of A' for R_{max} = 4.0 are essentially independent of the particular distribution rate, thus supporting the theoretical development in Appendix A.

(U)The deduced values of B are plotted in Fig. 2-20 for all four cases, and none save the quadratic distribution previously studied seems to reach a threshold level. At a sheet width of 1.5λ, the widest used in the analysis, the trailing edge components are decaying and finding their threshold levels would require sheets ranging from 1.8λ to 4.0λ wide, as judged from extrapolations of the behavior depicted. The linear and cubic distributions both exhibit slight undulations, suggesting either that the correct value of A' has not been extracted from the spiral plots or that A' is not constant, perhaps being weakly dependent upon ℓ.
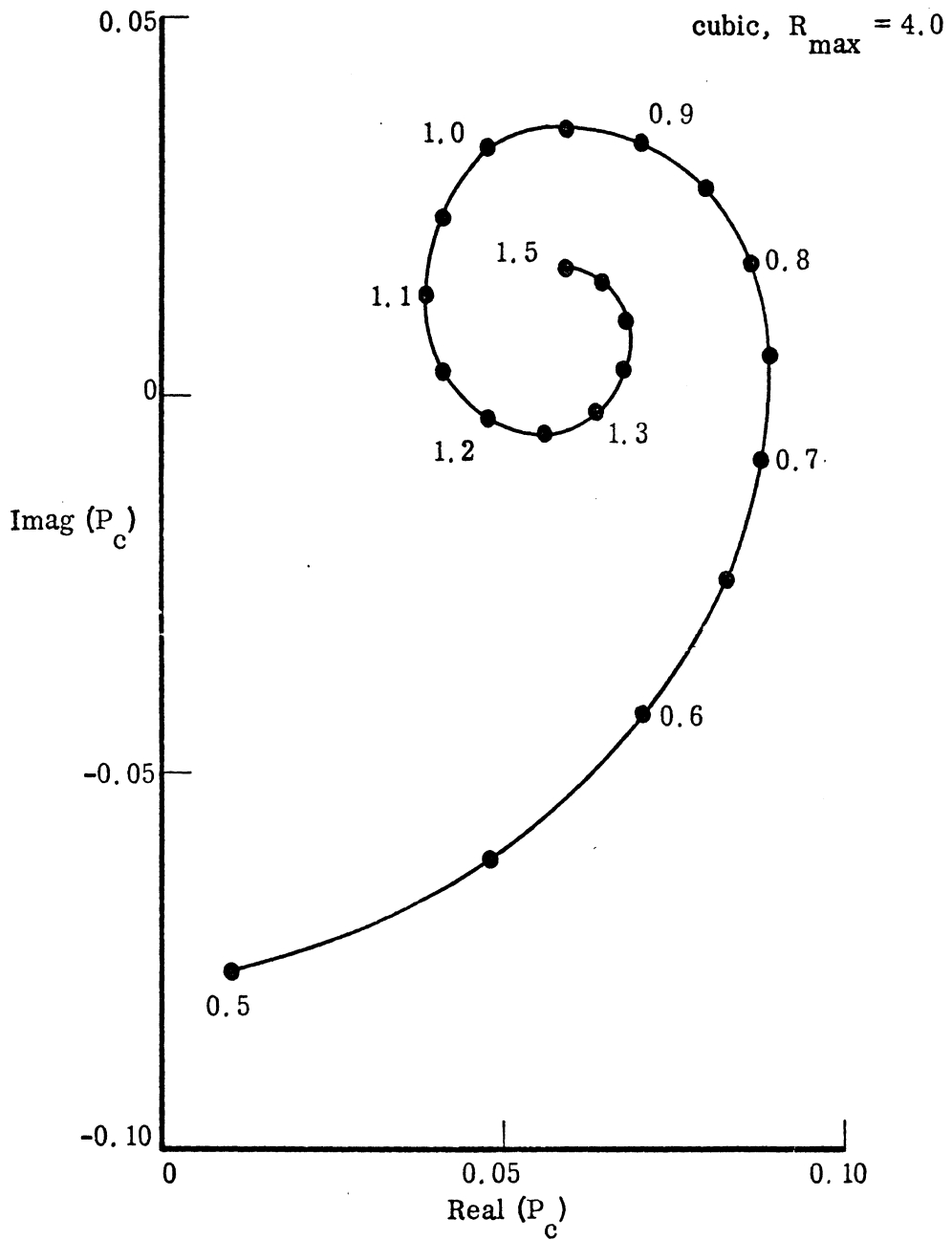
(U)The trailing edge contributions are replotted in Fig. 2-21 in the form of radar cross sections. The logarithmic scale tends to emphasize the smaller
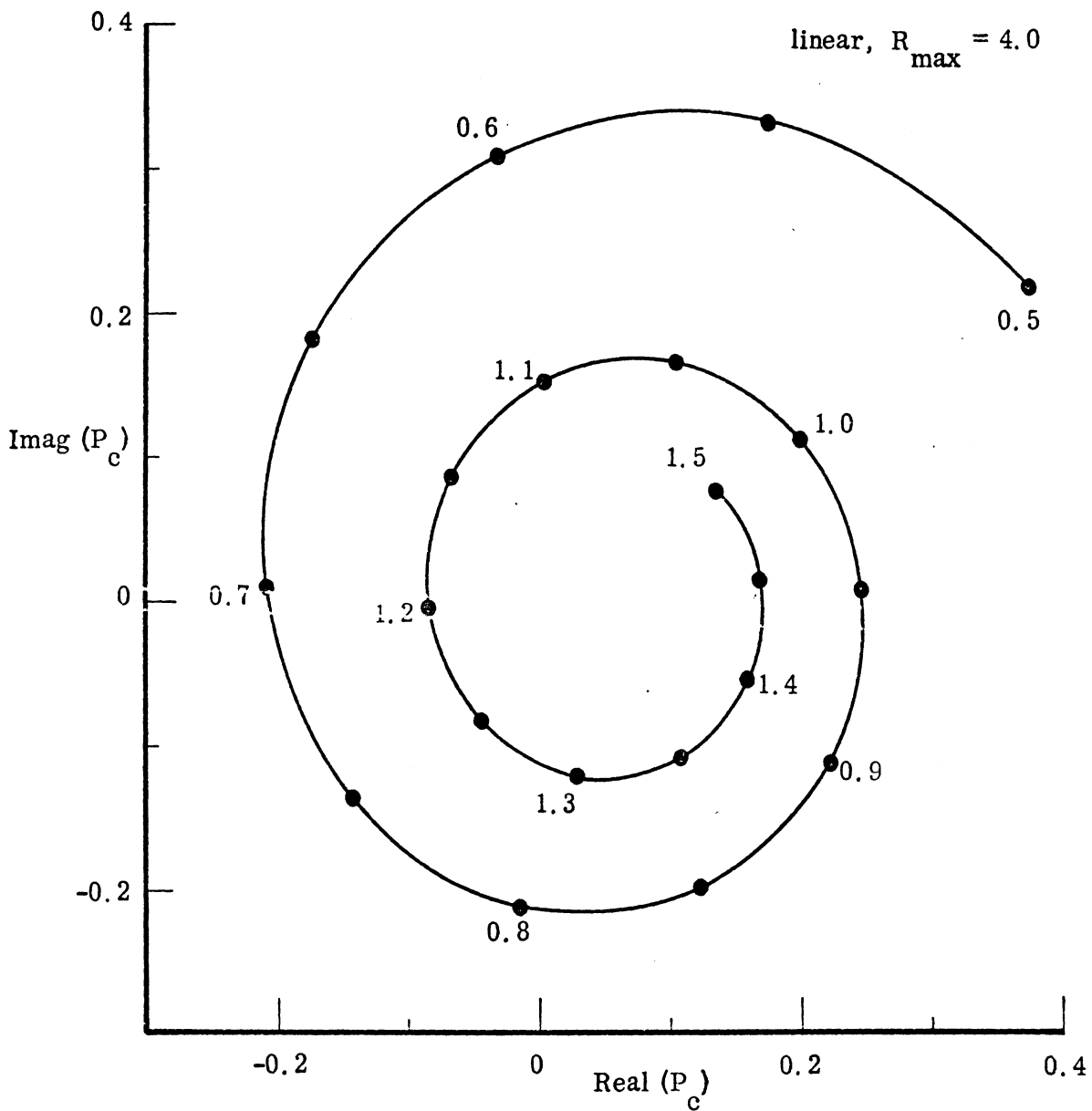
(U) FIG. 2-17: Plot of P_c for linear distribution, $R_{max} = 4.0$.
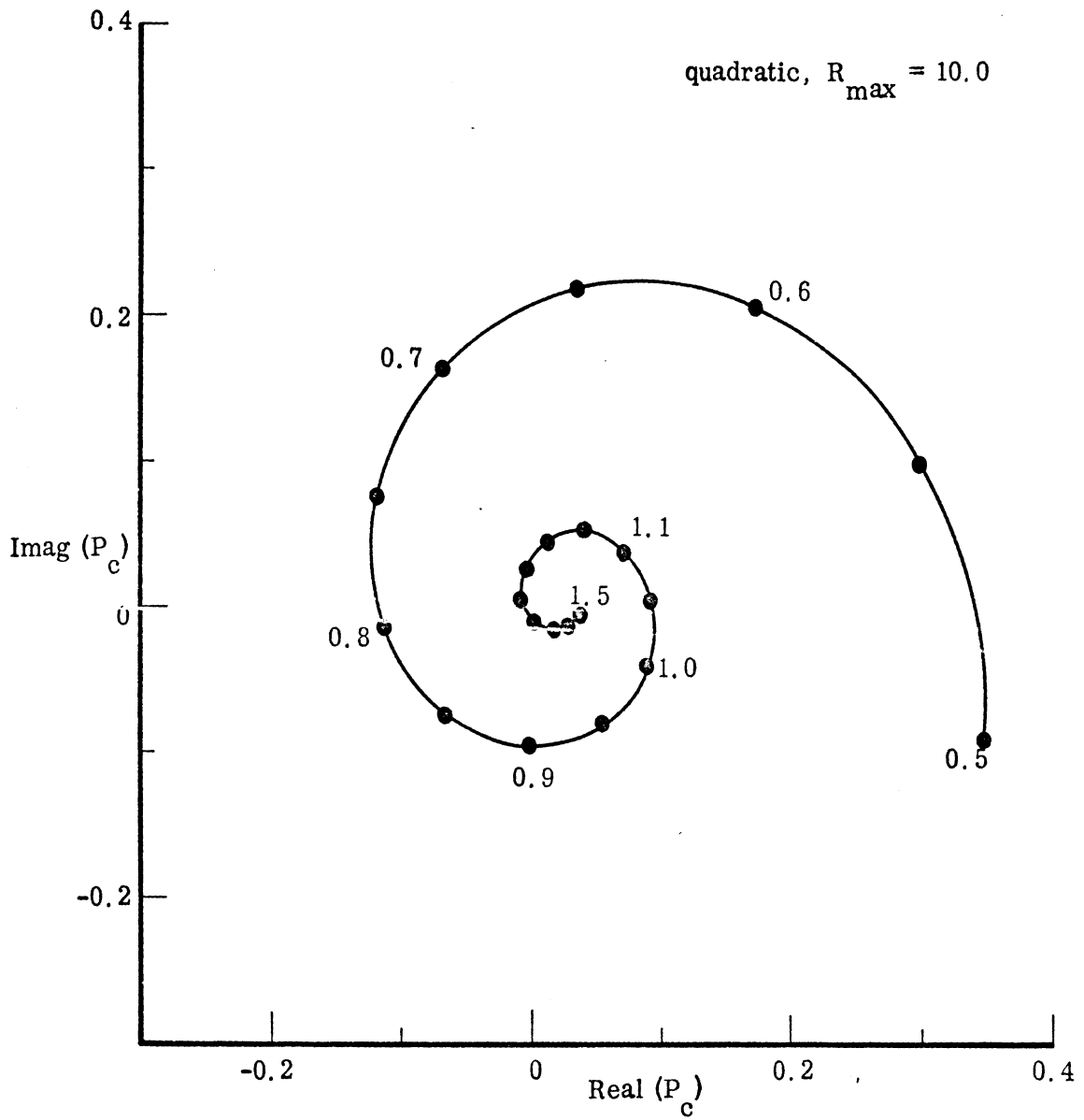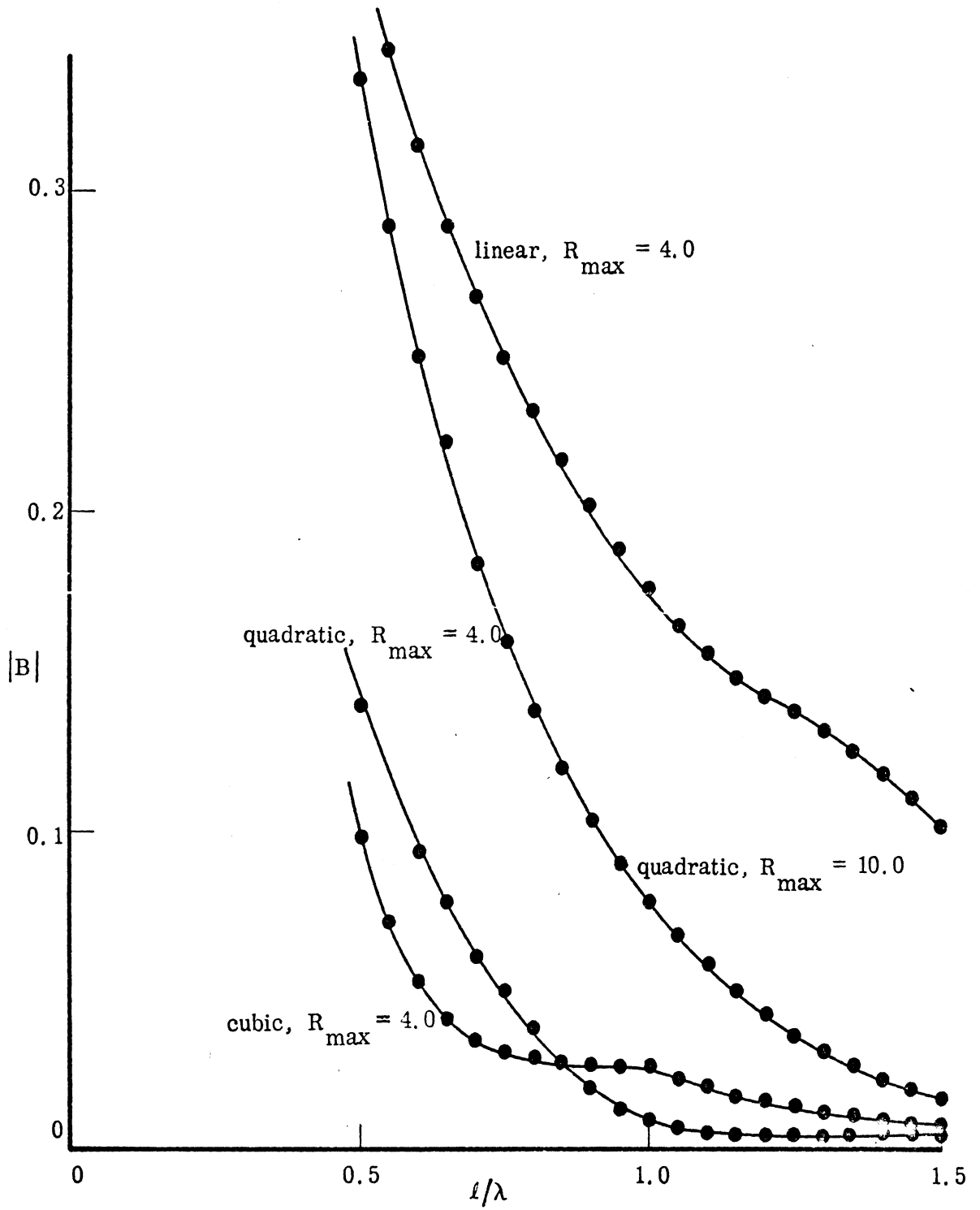
(U) FIG. 2-18: Plot of P_c for quadratic distribution, $R_{max} = 10.0$.

(U)FIG. 2-19: Plot of P_c for cubic distribution, R_{max} = 4.0.

(U)FIG. 2-20: Magnitudes of the trailing edge contributions.

MISSING
PAGE

MISSING
PAGE
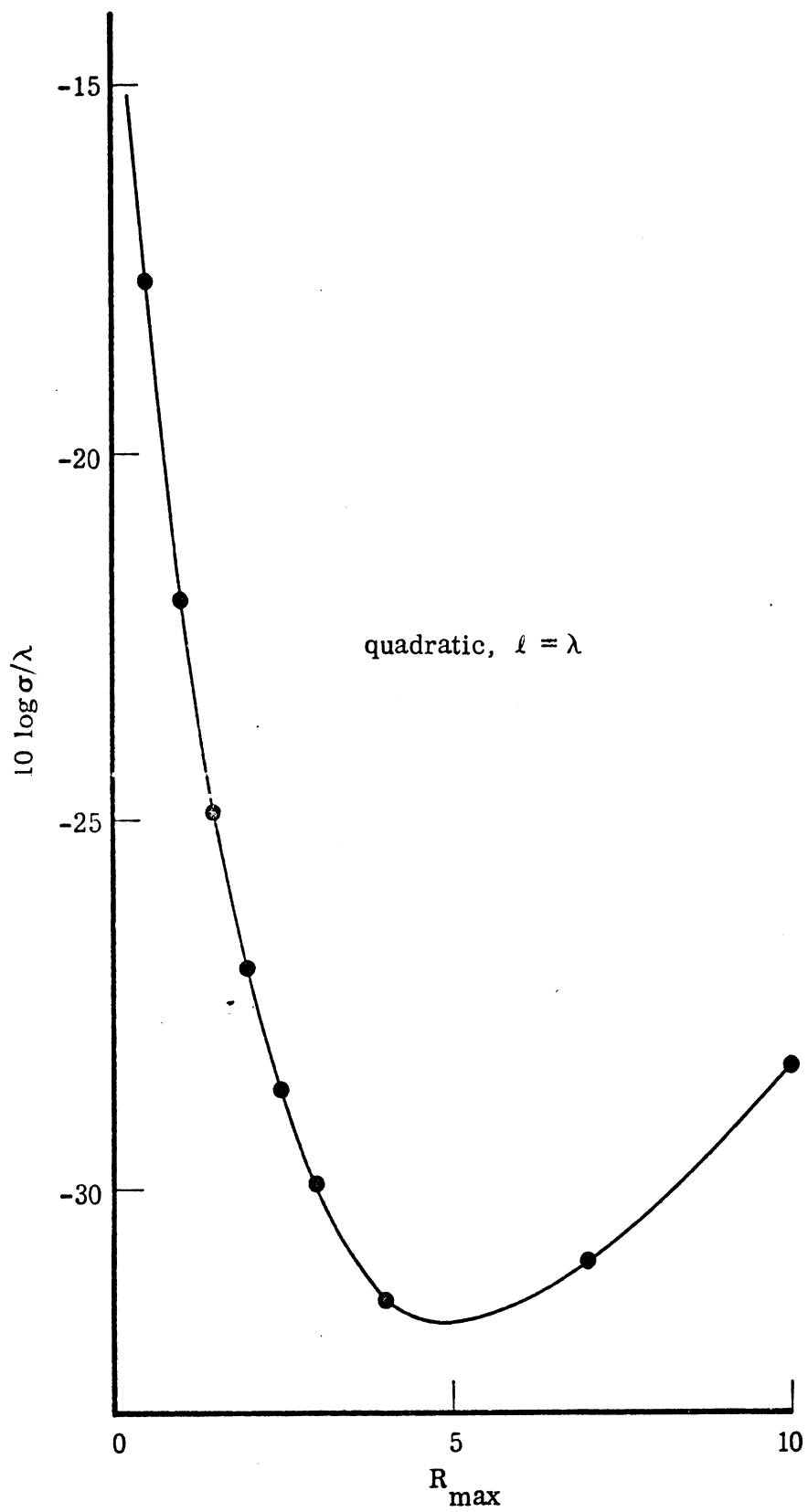
(U) FIG. 2-22: Optimization for fixed sheet width, quadratic distribution.
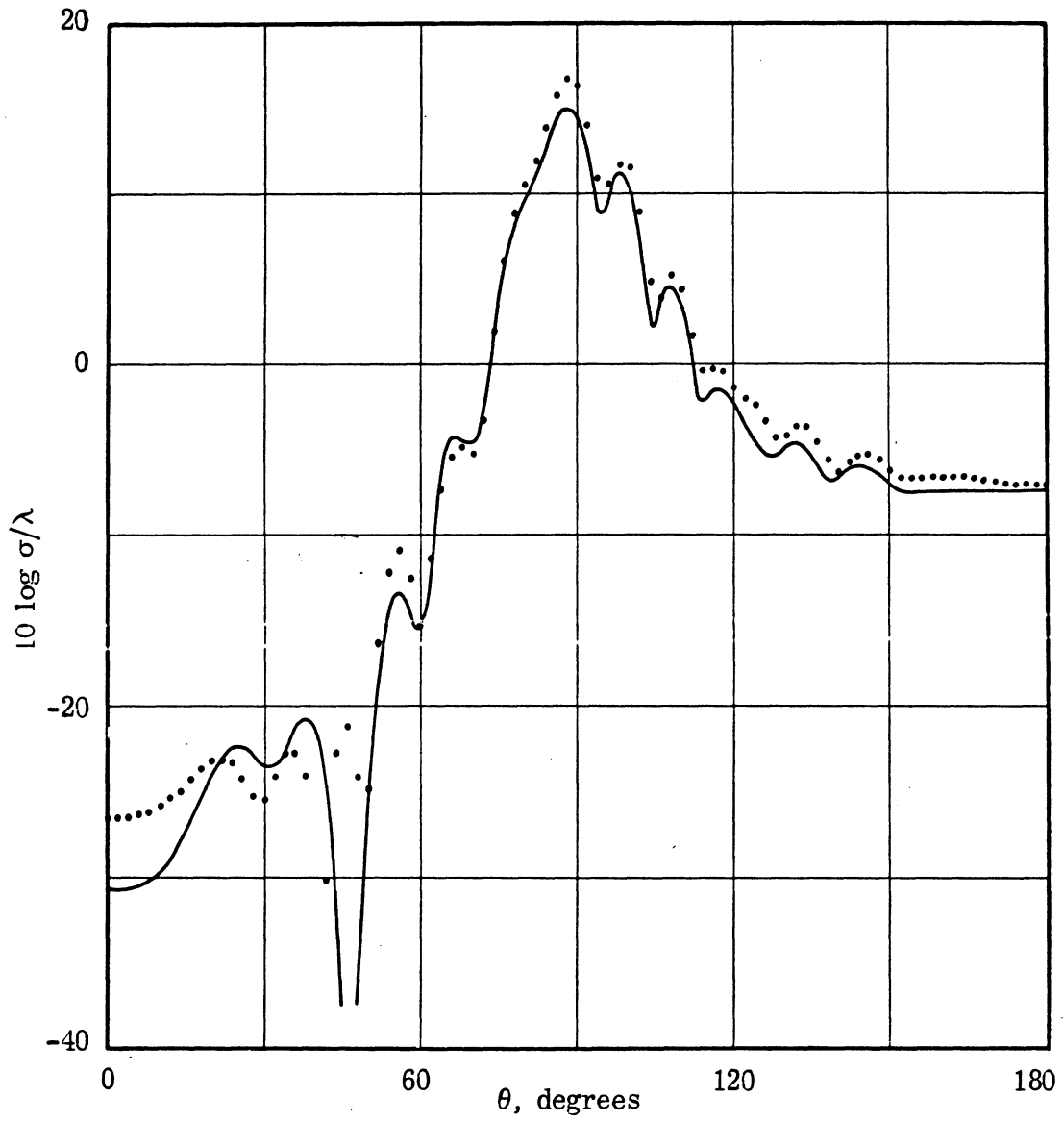
MISSING PAGE

MISSING
PAGE

MISSING
PAGE

MISSING
PAGE

MISSING
PAGE

MISSING
PAGE

MISSING
PAGE

MISSING
PAGE

(U)FIG. 2-28: Comparison of computed (———) and measured (• • •) patterns
of an edge-treated ogival cylinder.

MISSING
PAGE

MISSING
PAGE

MISSING
PAGE

remain, however, sufficient time to study the effectiveness of magnetic sheets placed ahead of the leading edge (or behind the trailing edge) of a metallic body—instead of on the surface, as was initially planned—and the results of this investigation are described in Sections 3.3 through 3.6 below. Before documenting the study, however, we first give the reader a glimpse of the nature of the program and its capabilities.

3.2 Program RAMVS

(U) The generalized program has been dubbed RAMVS and it solves the two-dimensional integral equations for the currents induced upon the surfaces of cylindrical bodies and thin sheets. The fields on the surfaces of solid bodies are assumed to satisfy an impedance boundary condition and the sheets are assumed to be electrically or "magnetically" resistive. Electric and magnetic sheets can be superposed and, if their resistivities are properly chosen, can be used to model the effect of a layer of absorbing material having arbitrary permittivity and permeability. The program reduces the integral equations to a system of simultaneous linear equations, solves for the unknown currents, and from these computes the far field scattering pattern. The program has been thoroughly described in the second Interim Report issued during this contract (Liepa, et al., 1974).

(U) Since RAMVS was designed as a research tool, and since electrically resistive sheets proved to be successful edge treatments via programs REST, RISK and RASP, it was natural to extend the concept of resistive sheets to the magnetic case as well. Although purely magnetic sheets do not exist in the physical sense, they are as amenable to mathematical treatment as are electric sheets, and the specification of a single parameter (resistivity) considerably simplifies the search for desirable sheet properties in reducing non-specular scattering. The electric and magnetic resistivities R and R^* can be related to the properties of physical materials by means of the expressions

$$R = \frac{iZ_0}{k\Delta(\epsilon_r - 1)} \quad , \qquad R^* = \frac{i}{Z_0 k\Delta(\mu_r - 1)} \qquad (3.1)$$

where Δ is the sheet thickness, k is the free space wave number, Z_0 is the impedance of free space and ϵ_r and μ_r are the permittivity and permeability of the sheet material, which may be complex.

(U) Thus, if a favorable configuration of sheets and resistance variations along the sheets can be found, then (3.1) can be used to deduce the characteristics of actual materials required to do so. Observe that, since the layer thickness is a factor influencing the effective resistivity, many combinations of electrical and dimensional properties can lead to the same value. On the other hand, given the properties of a thin layer of absorber, eqs. (3.1) can be used to estimate effective resistivities and the program could then be run to predict the scattered patterns. This was in fact done, and comparisons of computed and measured patterns are given in Figs. 3-1 through 3-4.
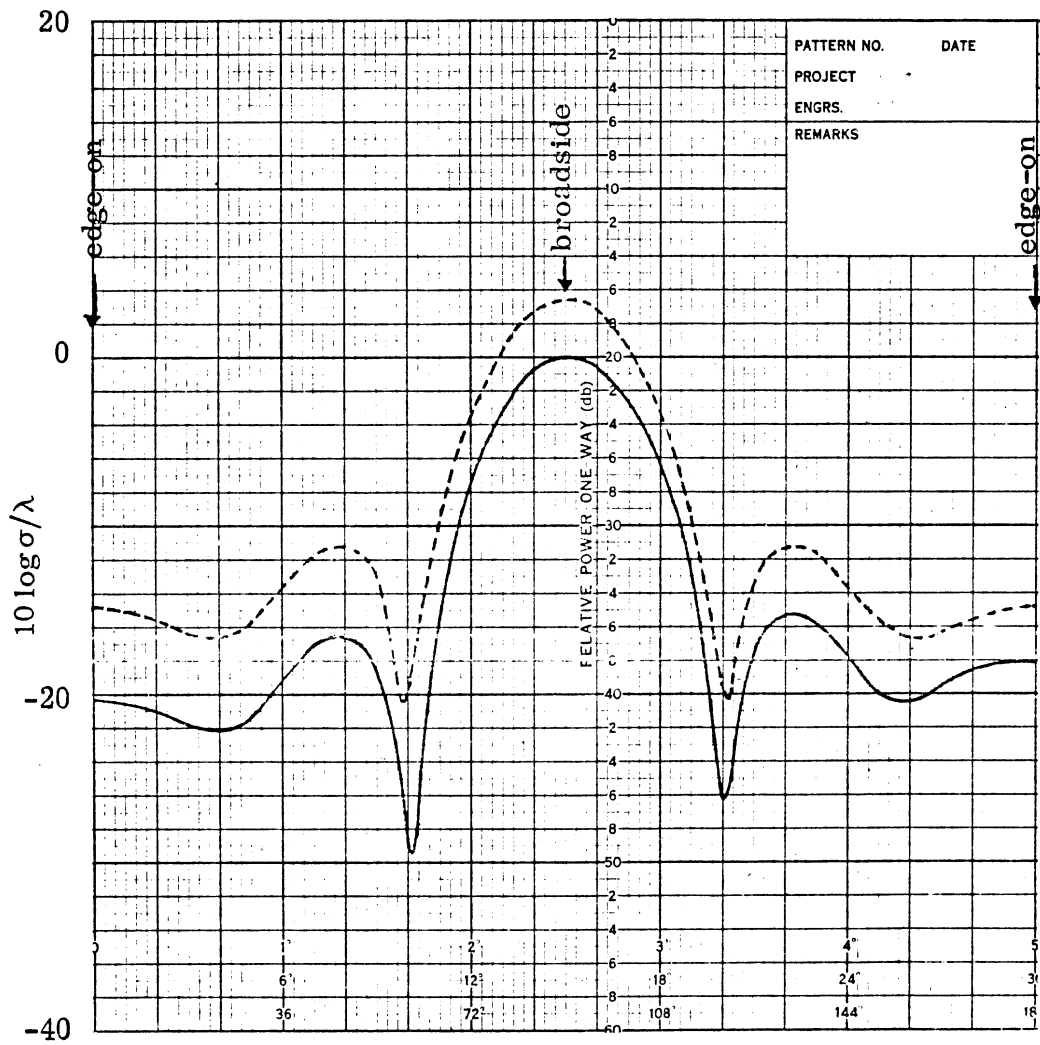
(U) The measured patterns are represented by the solid traces and were supplied by courtesy of the Air Force Avionics Laboratory. Figures 3-1 and 3-2 were for a strip of Emerson and Cuming LS-26 absorber 0.125 inch thick, 18 inches long and 1 wavelength wide at the measurement frequency (7.5 GHz). The relative permittivity of this material was measured by AFAL and reported to be

$$\epsilon_r = 3.55 + i4.20$$

at 7.5 GHz, the imaginary part being positive in accordance with the $e^{-i\omega t}$ time convention. The normalized resistivity is complex and from eqs. 3.1,

$$R = 0.34882 + i0.21178 .$$

Thus, using this value of R and omitting the need for a magnetic component to simulate the absorber, the computed data were obtained and plotted as the dashed lines. The measured (three-dimensional) cross sections were converted to the two-dimensional values via the expressions given in Appendix C of Knott, et al. (1973).

20

0

−20

−40

$10 \log \sigma/\lambda$

edge on

broadside

edge-on

edge-on

RELATIVE POWER, ONE WAY (db)

PATTERN NO. DATE
PROJECT
ENGRS.
REMARKS

(U) FIG. 3-1: Comparison of measured (——) and computed (- - -)
patterns of an isolated strip of LS-26 material for
vertical (E) polarization.
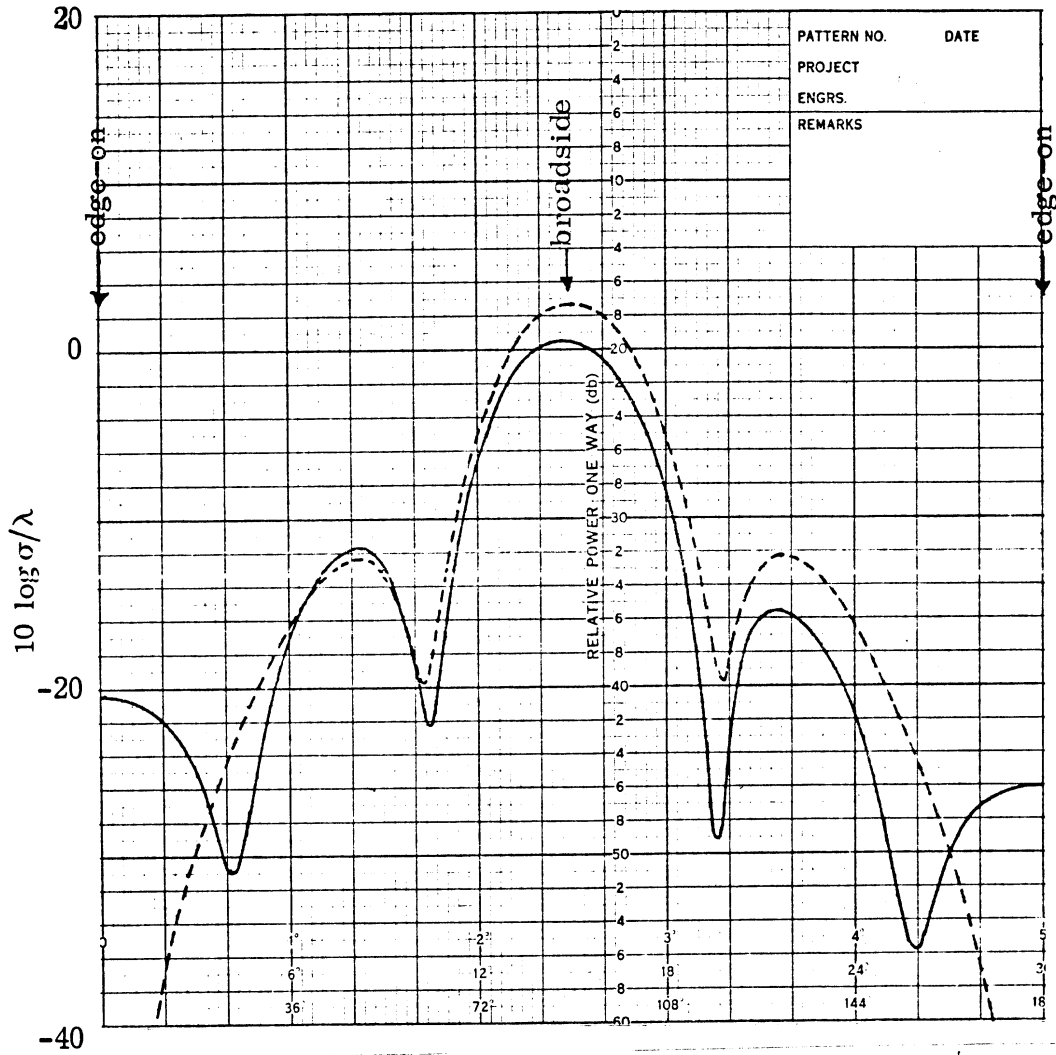
(U) FIG. 3-2: Comparison of measured (——) and computed (- - -) patterns of an isolated strip of LS-26 material for horizontal (H) polarization.

56

(U) Figure 3-1 shows the results for vertical polarization (electric field parallel to the edges), with edge-on incidence occurring at $\theta = 0^\circ$, 180° on the chart. The computed pattern lies above the measured one by approximately 4 dB, and the discrepancy at broadside (normal) incidence is about 3.3 dB. Both the measured and computed data have the same form, with peaks and nulls located at the same angular positions, and if it were not for the nearly constant 4 dB difference between them, the fit would be remarkable. The error may be due to improper calibration, an inadequacy of eqs. (3.1) or possibly differences between the electrical and physical properties of the sample whose pattern was measured and the samples used to obtain the electrical characteristics.

(U) Figure 3-2 shows the result for horizontal polarization for the LS-26 material and except for the regions near edge-on incidence, the agreement can be seen to be somewhat better than for vertical polarization. At edge-on incidence the predicted values go to zero ($-\infty$ dB), whereas the measured value is only some 25 to 30 dB below the broadside level. This represents a failure of the thin sheet approximation, since an infinitesimally thin electric sheet is truly invisible when seen at edge-on incidence by an H-polarized wave.

(U) Figures 3-3 and 3-4 show the comparison between measured and computed results for SF-11, a magnetic absorber also marketed by Emerson and Cuming. This material had the same length and width as the LS-26 sample, but was thinner, being only 0.043 inch thick. based upon measurements of the permittivity and permeability of other samples of the SF composition,

$$\epsilon_r = 12.0 + i0 \quad , \qquad \mu_r = 2.0 + i1.2 \quad ,$$

and the electric and magnetic resitivities specified on input to the program were therefore

$$R = i0.5295 \quad , \qquad R^* = 2.8646 + i2.3872.$$

57
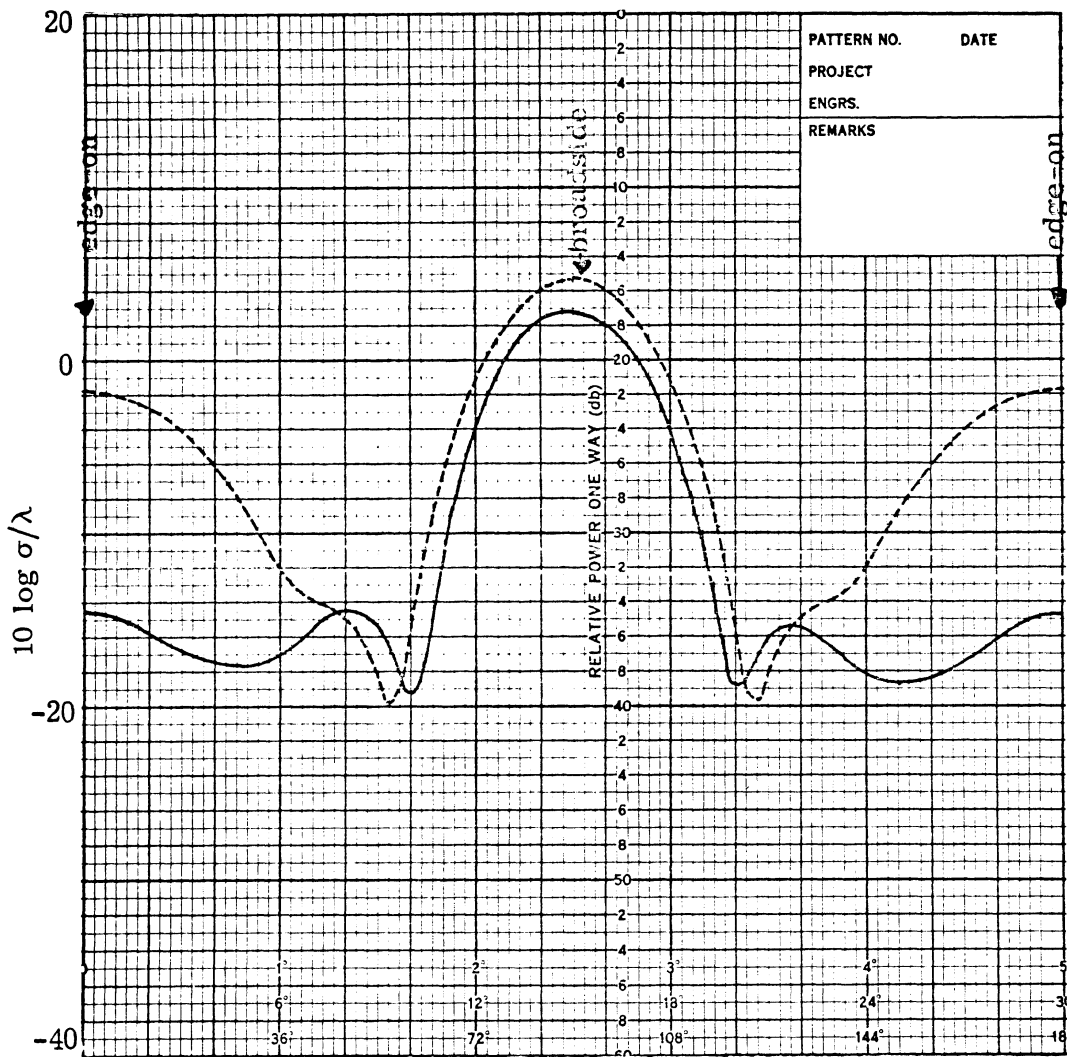
(U)FIG. 3-3: Comparison of measured (——) and computed (- - -)
patterns of an isolated strip of SF-11 material for
vertical (E) polarization.
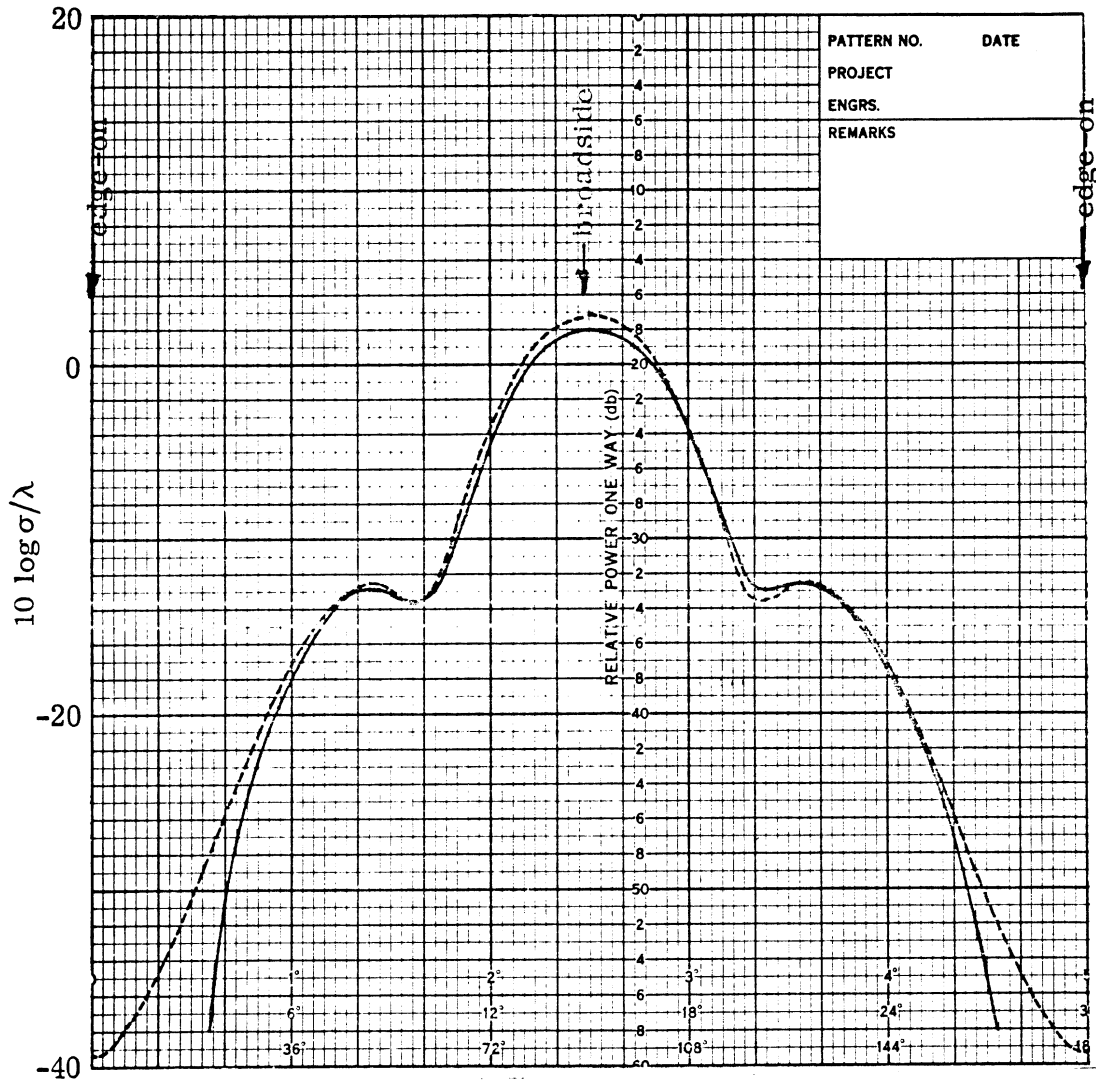
(U)FIG. 3-4: Comparison of measured (——) and computed (- - -) patterns of an isolated strip of SF-11 material for horizontal (H) polarization.

MISSING
PAGE

MISSING
PAGE

MISSING
PAGE

MISSING
PAGE

MISSING
PAGE

MISSING
PAGE

MISSING
PAGE

MISSING
PAGE

MISSING
PAGE

MISSING PAGE

MISSING
PAGE

MISSING
PAGE

(U)FIG. 3-12: Edge-on returns for metallic wedges.

wave at edge-on incidence, while a wedge is not, and the scattering we must suppress is therefore a consequence of the fact that 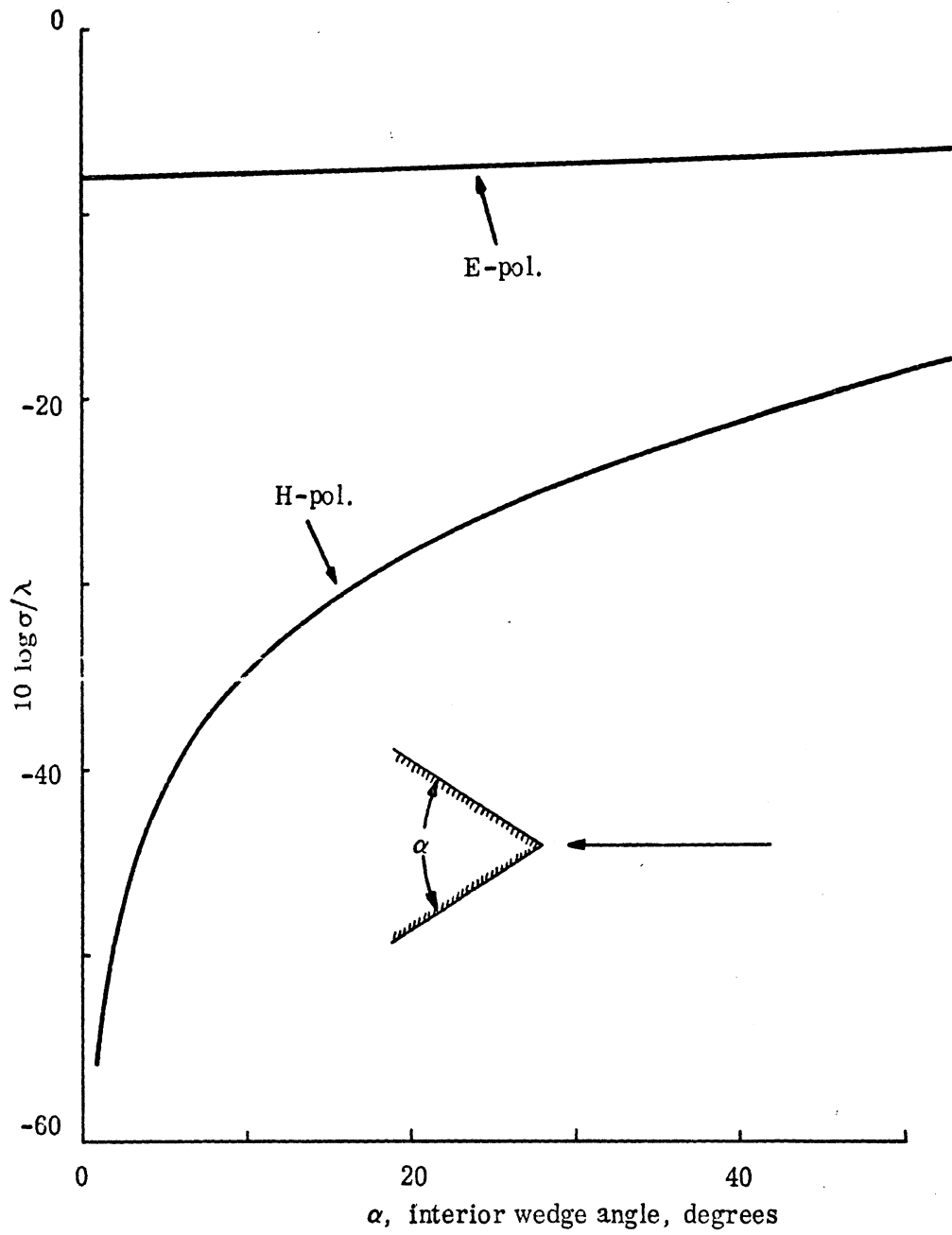the edge of the body is wedge-like. The rapid change in the edge-on return with increasing wedge angle is illustrated in Fig. 3-12 and it is apparent that the leading edge of the ogival cylinder would have a contribution of very nearly the target goal of -37 dBλ if the interior wedge angle could be reduced to 8 degrees. However, although this could be done without the use of magnetic sheets, the edge reverts to a trailing edge when the cylinder is viewed from the opposite direction. Thus, narrowing the wedge angle in order to reduce the leading edge return would still require that the edge be treated to suppress the strong travelling wave lobes that result when it becomes a trailing edge.

(U) A true knife edge can be generated by fairing the body profile into a concave shape, as was discussed in Section 2.6 for E-polarization, and such a geometry is sketched in Fig. 3-13(a). In order to provide a possible absorption mechanism for

a)

b)
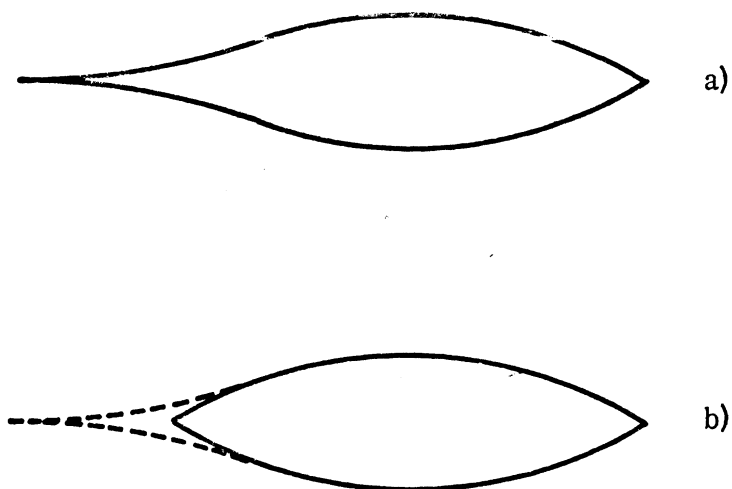
(U) FIG. 3-13: Faired metallic body (a), and body with faired magnetic sheet (b).

the travelling waves launched toward this knife edge from the opposite end of the body, we instead permitted the fairing to be made of magnetic sheets, thus forming the "shield" shown by the dashed lines in Fig. 3-12(b). The magnetic resistance

MISSING
PAGE

MISSING
PAGE

MISSING
PAGE

MISSING
PAGE

MISSING
PAGE

MISSING
PAGE

MISSING
PAGE

MISSING
PAGE

MISSING
PAGE

MISSING
PAGE

MISSING
PAGE

MISSING
PAGE

MISSING
PAGE

MISSING
PAGE

APPENDIX A

DIFFRACTION BY IMPEDANCE HALF PLANES

When illuminated by a plane wave at edge-on incidence, a sheet satisfying an impedance boundary condition is mathematically indistinguishable from a resistive sheet, and this fact has been of considerable value in understanding the scattering from resistive sheets. Since an exact solution is available for a constant impedance half plane, an expression for the edge diffraction coefficient can be obtained and then used to estimate the edge-on backscattering from an electric resistive sheet. The estimates agree quite well with numerical data, even for narrow sheets having rapid variations in resistance. However, the more recent studies described in Chapter II revealed a slight discrepancy which prompted a closer examination of both the surface and far scattered fields of a constant impedance half plane.

Our interest, then, is primarily in the case of an impedance half plane illuminated at edge-on incidence by a plane wave whose electric field is parallel to the edge. The magnetic current supported by the impedance half plane is identically zero in this case and the (remaining) electric current is analogous to that associated with an electric resistive sheet, even for oblique angles of incidence. Since Senior's treatment (1952) permits us to separate the effects of electric and magnetic currents, it is possible to obtain the edge diffraction coefficients for a resistive sheet for arbitrary incidence.

Unfortunately, Senior's results are given in terms of certain "split" functions which are much less convenient to use than the expressions of Maliuzhinets (1959), and it is therefore advantageous to explore the connection between them. This is done in Section A. 1. We then examine in Section A. 2 the electric surface field on the impedance half plane with emphasis on the region near the edge, and in Section A. 3 we derive an expression for the bistatic edge diffraction coefficient for a resistive sheet. Finally in Section A. 4 we examine an impedance half plane over which the impedance varies, but the variation is such that an exact solution of the diffraction problem is still obtainable.

A. 1 The "Split" Functions

For an E-polarized plane wave incident on a half plane of (constant) surface impedance η, the surface and far fields can be expressed in terms of the split functions $K_+(\xi)$ and $K_-(\xi)$ given in eqs. (21) and (20) of Senior (1952). Since

$$K_-(\xi) = \left(\eta + \frac{k}{\sqrt{k^2 - \xi^2}}\right) K_+(\xi) \tag{A. 1}$$

and

$$K_+(\xi) K_-(-\xi) = 1 \ , \tag{A. 2}$$

it is sufficient to consider only $K_+(\xi)$; and if, for simplicity, we write

$$\xi = k \cos \theta \ , \qquad \text{implying} \qquad \sin^{-1} \frac{\xi}{k} = \frac{\pi}{2} - \theta$$

and

$$\eta = \sec \chi \ , \qquad \text{implying} \qquad \sqrt{1 - \eta^2} = -i \tan \chi \ ,$$

eq. (21) becomes

$$K_+(k \cos \theta) = \left\{\frac{\cos \chi (1 + \cos \theta)}{\cos \chi + \sin \theta}\right\}^{1/2} \left\{\frac{\sin \chi - \cos \theta}{\sin \chi + \cos \theta}\right\}^{\chi/2\pi} \left\{\frac{\cos \chi - \sin \theta}{\cos \chi + \sin \theta}\right\}^{(\frac{2\theta}{\pi} - 1)/4}$$

$$\exp\left\{\frac{1}{2\pi} \int_0^{\frac{\pi}{2} - \theta} \log\left(\frac{\cos \chi - \cos s}{\cos \chi + \cos s}\right) ds\right\} \ . \tag{A. 3}$$

Integration by parts applied to the integral in (A. 3) yields an explicit term which cancels the third factor on the right hand side, and the second factor can be combined with the new integral to simplify it still further. As a result of these manipulations,

$$K_+(k\cos\theta) = \left\{\frac{\cos\chi(1+\cos\theta)}{\cos\chi+\sin\theta}\right\}^{1/2} \exp\left\{-\frac{1}{2\pi}\left(\int_0^{\frac{\pi}{2}-\theta-\chi} + \int_0^{\frac{\pi}{2}-\theta+\chi}\right)\frac{u\,du}{\sin u}\right\}.$$

(A. 4)

Maliuzhinets (1959) defines a meromorphic function $\psi_\pi(\beta)$ one of whose representations is

$$\psi_\pi(\beta) = \left(\frac{\sqrt{2}\cos\frac{\beta}{2}+1}{\sqrt{2}+1}\right)^{1/2}\left(\frac{e^{2b}}{1+\sin\beta}\right)^{1/8}\exp\left\{-\frac{1}{4\pi}\int_0^{\frac{\pi}{2}-\beta}\frac{u\,du}{\sin u}\right\}$$

(A. 5)

where $b = \dfrac{2}{\pi}\kappa$ with $\kappa = 0.9159656\ldots$ (Catalan's constant). In particular,

$$\psi_\pi(\pi/2) = \left(\frac{2}{\sqrt{2}+1}\right)^{1/2}\left(\frac{e^{2b}}{2}\right)^{1/8}$$

(A. 6)

and thus

$$\frac{\psi_\pi(\beta)}{\psi_\pi(\pi/2)} = \left(\frac{\sqrt{2}\cos\frac{\beta}{2}+1}{2}\right)^{1/2}\left(\frac{2}{1+\sin\beta}\right)^{1/8}\exp\left\{-\frac{1}{4\pi}\int_0^{\frac{\pi}{2}-\beta}\frac{u\,du}{\sin u}\right\}.$$ (A. 7)

Comparison of (A. 4) and (A. 7) now shows that

$$K_+(k\cos\theta) = \frac{2\{2\cos\chi(1+\cos\theta)\}^{1/2}}{\left(\sqrt{2}\cos\frac{\theta+\chi}{2}+1\right)\left(\sqrt{2}\cos\frac{\theta-\chi}{2}+1\right)}\left\{\frac{\psi_\pi(\theta+\chi)}{\psi_\pi(\pi/2)}\cdot\frac{\psi_\pi(\theta-\chi)}{\psi_\pi(\pi/2)}\right\}^2,$$

(A. 8)

and as a special case

$$K_+(k) = \frac{4(\cos\chi)^{1/2}}{\left(\sqrt{2}\cos\frac{\chi}{2}+1\right)^2}\left\{\frac{\psi_\pi(\chi)}{\psi_\pi(\pi/2)}\right\}^4,$$

(A. 9)

$\psi_\pi(\beta)$ being an even function of β.

Equation (A. 9) can be used to determine the behavior of $K_+(\xi)$ for large $|\xi|$, $0 < \arg \xi < \pi$. For this purpose, let $\theta = i\gamma$ where γ is real and will be allowed to approach infinity. From one of the alternative representations of $\psi_\pi(\beta)$, we have

$$\psi_\pi(\beta) = \left(\frac{\sqrt{2} \cos \frac{\beta}{2} + 1}{\sqrt{2} + 1} \right)^{1/2} (\cos \beta)^{-1/8} \exp \left\{ - \frac{1}{4\pi} \int_0^\beta \frac{v\, dv}{\cos v} \right\} \qquad \text{(A. 10)}$$

(Bowman, 1967), and since

$$\int_0^{i\infty} \frac{v\, dv}{\cos v} = -\pi b \ ,$$

it follows that

$$\psi_\pi(\beta) = \left(\frac{\sqrt{2} \cos \frac{\beta}{2} + 1}{\sqrt{2} + 1} \right)^{1/2} (\cos \beta)^{-1/8} \exp \left\{ \frac{b}{4} + \frac{1}{4\pi} \int_\beta^{i\infty} \frac{v\, dv}{\cos v} \right\} \ .$$

Hence, from (A. 6)

$$\frac{\psi_\pi(\beta)}{\psi_\pi(\pi/2)} = \left(\frac{\sqrt{2} \cos \frac{\beta}{2} + 1}{2} \right)^{1/2} \left(\frac{2}{\cos \beta} \right)^{1/8} \exp \left\{ \frac{1}{4\pi} \int_\beta^{i\infty} \frac{v\, dv}{\cos v} \right\} \qquad \text{(A. 11)}$$

and for $\gamma \gg 1$,

$$\frac{\psi_\pi(\theta + \chi)}{\psi_\pi(\pi/2)} \sim \frac{1}{\sqrt{2}} \exp \left\{ \frac{\gamma}{8} - \frac{i\chi}{4} \right\} \ ,$$

implying

$$\frac{\psi_\pi(\theta + \chi)}{\psi_\pi(\pi/2)} \cdot \frac{\psi_\pi(\theta - \chi)}{\psi_\pi(\pi/2)} \sim \frac{1}{2} e^{\gamma/4} \ .$$

When this is inserted into (A. 8) and the remaining trigonometrical factors approximated for $\gamma \gg 1$, we have

$$K_+(\xi) \sim (\cos\chi)^{1/2} = \eta^{-1/2} \quad , \qquad \xi \gg 1 \quad , \tag{A. 12}$$

valid for $\eta \neq 0$.

A.2 The Surface Field

The surface electric field E_z on a constant impedance half plane can be obtained by putting $\theta = 0$ in the general expression (Senior, 1952; eq. 34) for the diffracted field, but in the special case of edge-on incidence ($\alpha = \pi$), it proves more convenient to start with the total induced electric current

$$I_2(x) = H_x(x, +0) - H_x(x, -0) \quad .$$

Note that this is the negative of the current $J(x)$ computed in the electric resistive sheet program.

Since the magnetic current $I_1(x)$ is zero if $\alpha = \pi$, E_z is continuous across the half plane and from the boundary condition at the surface,

$$E_z(x) = \mp \eta Z_0 H_x(x, \pm 0)$$

implying

$$E_z(x) = -\frac{\eta}{2} Z_0 I_2(x) \quad . \tag{A. 13}$$

An expression for $I_2(x)$ is given in eq. (25) of Senior (1952) and when $\alpha = \pi$

$$I_2(x) = -\frac{2i}{\pi} Y_0 \int_{C'} \frac{K_+(k)}{K_+(k\cos\beta)} \frac{\cos^2\frac{\beta}{2}}{1+\eta\sin\beta} e^{ikx\cos\beta} d\beta$$

where C' is a steepest descent path through the saddle point $\beta = 0$. Hence, for $kx \gg 1$,

$$I_2(x) \sim -2Y_0 \sqrt{\frac{2}{\pi kx}} \exp\left(ikx + i\frac{\pi}{4}\right)$$

giving

$$E_z(x) \sim \eta \sqrt{\frac{2}{\pi kx}} \exp\left(ikx + i\frac{\pi}{4}\right) \quad , \tag{A. 14}$$

92

which has the form of an edge wave.

Of more direct interest, however, is the behavior of the surface field close to the edge, and this can be deduced from the properties of the Fourier transform $\bar{I}_2(\xi)$ of $I_2(x)$ for large $|\xi|$. Since

$$\bar{I}_2(\xi) = iY_0 \sqrt{2/\pi} \; \frac{1}{\xi-k} \; \frac{\sqrt{k^2-\xi^2}}{k+\eta\sqrt{k^2-\xi^2}} \; \frac{K_+(k)}{K_+(\xi)} \quad ,$$

eq. (A. 12) implies

$$\bar{I}_2(\xi) \sim i \; \frac{Y_0}{\xi} \; \sqrt{\frac{2}{\pi\eta}} \; K_+(k)$$

as $|\xi| \to \infty$. Hence

$$I_2(0) = -2Y_0 \eta^{-1/2} K_+(k)$$

and

$$E_z(0) = \eta^{1/2} K_+(k) \quad . \tag{A. 15}$$

Asymptotic approximations to $K_+(k)$ for large and small $|\eta|$ can be obtained from eq. (A. 18) using the results in eqs. (3. 12) and (3. 15) of Knott and Senior (1974). In particular, if $|\eta| \gg 1$,

$$K_+(k) \sim \eta^{-1/2} \exp\left(\frac{-1}{\pi\eta}\right)$$

and in this case

$$E_z(0) \sim \exp\left(\frac{-1}{\pi\eta}\right) \quad . \tag{A. 16}$$

The values predicted by eq. (A. 16) are in excellent agreement with data computed for resistive sheets having a quadratic variation of resistance. As an example, for $R_{max} = 4$ (at the front) the computed data show that $J(0) = 0.240 \exp(i9.9^\circ)$ for sheets of length ℓ, $0.7 \leq \ell/\lambda \leq 1.5$, and since $E_z = RJ$, it follows that

$$E_z(0) = 0.960 \exp(i9.9^\circ) \quad .$$

For comparison, eq. (A.16) with $\eta = 8$ gives

$$E_z(0) = 0.961 .$$

The magnitudes are virtually indistinguishable and though (A.16) does not explain it, the observed non-zero phase is equivalent to a displacement of the effective edge of the sheet by only $\lambda/36$ and can be attributed to the resistance variation in the vicinity of the edge (see Section A.4).

A.3 Edge Diffraction

The edge diffraction coefficient $P(\alpha, \theta)$, where α and θ are the angles of incidence and scattering, respectively, has been investigated by Knott and Senior (1974) for edge-on incidence ($\alpha = \pi$) starting with Bowman's expression (1967). An alternative approach leading to the same result is to use Senior's expression (1952),

$$P(\pi, \theta) = -\frac{i}{4} \cosec^2 \frac{\theta}{2} \frac{K_+(k)}{K_-(k \cos \theta)}$$

and hence, from eq. (A.2),

$$P(\pi, \pi-\theta') = -\frac{i}{4} \sec^2 \frac{\theta'}{2} K_+(k) K_+(k \cos \theta') \qquad (A.17)$$

where, for convenience, we have written $\theta' = \pi - \theta$. In particular, for backscattering ($\theta' = 0$),

$$P(\pi, \pi) = -\frac{i}{4} \left\{ K_+(k) \right\}^2 , \qquad (A.18)$$

i.e.,

$$P(\pi, \pi) = -i \frac{4 \cos \chi}{\left(\sqrt{2} \cos \frac{\chi}{2} + 1 \right)^4} \left\{ \frac{\psi_\pi(\chi)}{\psi_\pi(\pi/2)} \right\}^8 \qquad (A.19)$$

on using (A.9). If we now insert the expression for $\psi_\pi(\chi)/\psi_\pi(\pi/2)$ obtained from eq. (A.11) with $\beta = \chi$, $P(\pi, \pi)$ becomes

$$P(\pi,\pi) = -\frac{i}{2}\exp\left\{\frac{2}{\pi}\int_{\chi}^{i\infty}\frac{v\,dv}{\cos v}\right\} \tag{A.20}$$

in agreement with eq. (3.8) of Knott and Senior (1974).

For a perfectly conducting half plane, $\eta = 0$ and $\chi = i\infty$; consequently the integral is then zero and the diffraction coefficient reduces to the known value $-i/2$ for a metallic edge. If we normalize with respect to this, the resulting coefficient is

$$\tilde{P}(\pi,\pi) = \exp\left\{\frac{2}{\pi}\int_{\chi}^{i\infty}\frac{v\,dv}{\cos v}\right\}. \tag{A.21}$$

A tabulation of $\tilde{P}(\pi,\pi)$, evaluated for real η using a Gaussian quadrature method, is given in Table A-1 and these data are plotted in Fig. 2-7. The last column in Table A-1 lists the scattering length per wavelength,

$$\sigma/\lambda = \frac{2}{\pi}\left|P(\pi,\pi)\right|^2.$$

For bistatic scattering

$$\frac{P(\pi,\pi-\theta')}{P(\pi,\pi)} = \sec^2\frac{\theta'}{2}\frac{K_+(k\cos\theta')}{K_+(k)}$$

and hence, from (A.8) and (A.9),

$$\frac{P(\pi,\pi-\theta')}{P(\pi,\pi)} = \sec\frac{\theta'}{2}\frac{\sqrt{2}\cos\frac{\chi}{2}+1}{\sqrt{2}\cos\frac{\chi+\theta'}{2}+1}\frac{\sqrt{2}\cos\frac{\chi}{2}+1}{\sqrt{2}\cos\frac{\chi-\theta'}{2}+1}\left\{\frac{\psi_\pi(\chi+\theta')}{\psi_\pi(\chi)}\frac{\psi_\pi(\chi-\theta')}{\psi_\pi(\chi)}\right\}^2. \tag{A.22}$$

There is one consequence of this which is rather interesting and markedly simplifies the task of computing the bistatic scattering. If we denote by $Q(\chi)$ the expression (A.19) for the backscattering coefficient of a surface whose impedance is specified by the angle χ, we have

TABLE A-1: EDGE DIFFRACTION

η	$P(\pi, \pi)$	$10 \log \sigma/\lambda$
.01	.96070	-8.33
.02	.93112	-8.60
.03	.90545	-8.84
.04	.88240	-9.07
.05	.86131	-9.28
.06	.84180	-9.48
.07	.82360	-9.67
.08	.80652	-9.85
.09	.79041	-10.02
.1	.77517	-10.20
.2	.65551	-11.66
.3	.57209	-12.83
.4	.50918	-13.84
.5	.45956	-14.73
.6	.41919	-15.53
.7	.38561	-16.27
.8	.35717	-16.93
.9	.33275	-17.53
1.0	.31154	-18.10
2.0	.19100	-22.37
3.0	.13800	-25.18
4.0	.10808	-27.30
5.0	.088841	-29.01
6.0	.075422	-30.43
7.0	.065528	-31.66
8.0	.057930	-32.73
9.0	.051912	-33.68
10.0	.047027	-34.53
20.0	.024231	-40.28
30.0	.016321	-43.76
40.0	.012305	-46.19
50.0	.0098744	-48.08
60.0	.0082459	-49.66
70.0	.0070785	-50.99
80.0	.0062007	-52.13
90.0	.0055166	-53.15

$$\left\{\frac{\psi_\pi(\chi)}{\psi_\pi(\pi/2)}\right\}^2 = \left(\frac{i}{4}\sec\chi\right)^{1/4}\left(\sqrt{2}\cos\frac{\chi}{2}+1\right)\left\{Q(\chi)\right\}^{1/4} \ ,$$

and on replacing χ by $\chi \pm \theta'$, the results can be inserted into eq. (A.22) to give

$$\frac{P(\pi, \pi-\theta')}{P(\pi, \pi)} = \sec\frac{\theta'}{2}\left\{\frac{\cos^2\chi}{\cos^2\chi-\sin^2\theta'}\frac{Q(\chi+\theta')}{Q(\chi)}\cdot\frac{Q(\chi-\theta')}{Q(\chi)}\right\}^{1/4} \ . \qquad (A.23)$$

which enables us to deduce the bistatic scattering from the backscattering coefficients for different surface impedances.

If the plane wave is incident at an oblique angle $(\alpha \neq \pi)$, an impedance half plane has a magnetic current as well as an electric one whereas a resistive half plane can support only the latter. Nevertheless, the electric current is the same for both structures and we can therefore deduce the diffraction coefficient for a resistive sheet by considering only the contribution of this current to the diffraction coefficient of an impedance half plane. From eq. (34) of Senior (1952), we now have that for a resistive sheet

$$P(\alpha, \theta) = \frac{i}{2}(\cos\alpha+\cos\theta)^{-1}\frac{K_+(-k\cos\alpha)}{K_-(k\cos\theta)} \ ,$$

implying

$$P(\alpha', \theta') = -\frac{i}{2}(\cos\alpha'+\cos\theta')^{-1}K_+(k\cos\alpha')K_+(k\cos\theta')$$

where $\alpha' = \pi-\alpha$. Comparison with eq. (A.17) shows

$$P(\alpha', \theta') = \frac{1}{2}\frac{(1+\cos\alpha')(1+\cos\theta')}{\cos\alpha'+\cos\theta'}\frac{P(\pi, \pi-\alpha')P(\pi, \pi-\theta')}{P(\pi, \pi)} \ . \qquad (A.24)$$

We can therefore obtain the bistatic coefficient for any angle of incidence from the coefficient for edge-on incidence $(\alpha' = 0)$, and hence, via eq. (A.23), from the backscattering coefficient for edge-on incidence. In particular, for backscattering $(\theta' = \alpha')$,

$$\frac{P(\alpha', \alpha')}{P(\pi, \pi)} = \left\{ \frac{1}{2} (1 + \sec \alpha') \frac{P(\pi, \pi - \alpha')}{P(\pi, \pi)} \right\}^2 \qquad (A.25)$$

which is a strikingly simple result.

A.4 Tapered Impedance Half Plane

With the growing importance of variable impedance or resistive sheets, it is of interest to re-examine those solutions for specific variations which were originally developed many years ago but which, at the time, seemed rather academic and devoid of practical applications. An example is the solution obtained by Shmoys (see Felsen, 1958) for a plane wave incident on a half plane having a particular type of impedance variation.

The method is an extension of one proposed by Lamb (1945). By separation of variables in a mixed coordinate system consisting of parabolic cylinder and Cartesian coordinates, it is possible to construct a solution of the wave equation satisfying the radiation condition and having certain constants still undetermined. Under normal circumstances these would be specified by the boundary conditions on the half plane, but instead of imposing the conditions at the outset, the constants can be used to see what boundary conditions can be satisfied by the solution.

By proceeding in this manner it can be shown that for a plane wave

$$u^i = e^{-ik(x \cos \alpha + y \sin \alpha)} \qquad (A.26)$$

incident on an opaque half plane $y = 0$, $x \geq 0$, a solution of the wave equation satisfying the radiation condition is

$$u = \frac{e^{-i\pi/4}}{\sqrt{\pi}} \left\{ e^{-ik\rho \cos(\theta - \alpha)} F\left(-\sqrt{2k\rho} \cos \frac{\theta - \alpha}{2} \right) + R e^{-ik\rho \cos(\theta + \alpha)} \right.$$

$$\left. \times F\left(-\sqrt{2k\rho} \cos \frac{\theta + \alpha}{2} \right) \right\} \qquad (A.27)$$

where R is a reflection coefficient and F is the Fresnel integral

$$F(\tau) = \int_{\tau}^{\infty} e^{i\mu^2} d\mu \ .$$

The requirement that the half plane be opaque has left only the one constant R undertermined. If $R = -1$, u is simply the total field E_z for an E-polarized plane wave $u^i = E_z^i$ incident on a perfectly conducting half plane. Similarly, if $R = 1$, $u = H_z$ is the H-polarized solution, whereas if R is left arbitrary, the solution is identical to that obtained by Raman and Krishnan (1927) for an imperfectly reflecting screen.

The edge diffraction coefficient implied by the field (A. 27) is

$$P(\alpha, \theta) = -\frac{i}{4} \left(\sec \frac{\alpha - \theta}{2} + R \sec \frac{\alpha + \theta}{2} \right) \ .$$

For edge-on incidence $(\alpha = \pi)$ this reduces to

$$P(\pi, \theta) = -\frac{i}{4} (1 - R) \csc \frac{\theta}{2} \tag{A. 28}$$

and since, for a perfectly conducting half plane, $I - R = \begin{Bmatrix} 2 \\ 0 \end{Bmatrix}$ for $\begin{smallmatrix} E \\ H \end{smallmatrix}$ -polarization, reduction of the E-polarized edge diffraction requires that $1 - R$ be small.

If u is identified with either E_z or H_z, it is found that u satisfies an impedance boundary condition at the surface, with

$$\eta_E = 1/\eta_H$$

as expected, and

$$\eta_E = \frac{1+R}{1-R} \left\{ \pm \sin\alpha + \frac{i}{\sqrt{2kx}} \sin\frac{\alpha}{2} \frac{e^{ikx(1+\cos\alpha)}}{F\left(\mp \sqrt{2kx} \cos\frac{\alpha}{2}\right)} \right\} \tag{A. 29}$$

where the upper (lower) signs refer to the upper (lower) surface. For a half plane with the impedance (A. 29), the expression for u given in eq. (A. 27) is an exact solution for the diffraction of the plane wave (A. 26). In the particular case of edge-on incidence,

$$\eta_E = \sqrt{\frac{\pi k x}{2}} \; e^{-i\pi/4} \frac{1+R}{1-R} \quad . \tag{A.30}$$

This is zero when $x = 0$, so that the edge of the half plane looks perfectly conducting for all $R \neq 1$, but away from $x = 0$ the rate at which the impedance builds up increases as $R \rightarrow 1$. As R approaches this limit, however, $P(\pi, \theta) \rightarrow 0$. Such behavior is characteristic of a constant impedance half plane as $\eta \rightarrow \infty$ and demonstrates that the edge diffraction coefficient is determined not by the impedance at the edge itself, but rather by an average impedance in the vicinity of the edge.

By solving eq. (A.30) for R and substituting this into eq. (A.27) with $\theta = \pi$, we obtain

$$P(\pi, \pi) = -\frac{i}{2} \left(1 + \frac{\eta_E \, e^{i\pi/4}}{\sqrt{\frac{\pi k x}{2}}} \right)^{-1} , \tag{A.31}$$

and though this is rather meaningless as it stands, it does enable us to find the equivalent constant impedance for backscattering at edge-on incidence. For a half plane of constant impedance η, an expression for $P(\pi, \pi)$ is given in eq. (A.20) and approximations for large and small impedances were presented in Knott and Senior (1974; eqs. 3.12 and 3.15). Since these are valid for complex as well as real η, it follows that if $\eta = a e^{-i\pi/4}$ with a real,

$$P(\pi, \pi) \simeq -\frac{i}{2} \exp\left\{ -\frac{a\sqrt{2}}{\pi} \left(1 - \log \frac{a}{2} + \frac{\pi}{4} \right) \right\} \exp\left\{ i \, \frac{a\sqrt{2}}{\pi} \left(1 - \log \frac{a}{2} - \frac{\pi}{4} \right) \right\}$$

for $a \lesssim 1$, and

$$P(\pi, \pi) \simeq -\frac{i}{4a} \exp\left(-\frac{\sqrt{2}}{\pi a} \right) \exp\left\{ i \left(\frac{\pi}{4} - \frac{\sqrt{2}}{\pi a} \right) \right\}$$

for $a \gtrsim 1$. By equating these to the expression for $P(\pi, \pi)$ in eq. (A.31) we can determine the distance x at which the variable impedance (A.30) must be read to produce a diffraction coefficient having the same magnitude as a half plane with

constant impedance. The detailed calculations can be found in Senior (1973) and show that for all a $\gtrsim 0.4$, implying R $\gtrsim -0.1$, equivalence is obtained by taking x $= 1/2\pi k$. This can be interpreted as a displacement of the effective edge of the variable impedance half plane. In spite of the fact that the impedance variation is quite different from that used in the electrically resistive sheet study, it is interesting to note that the displacement is the same as that suggested by the surface field data discussed in Section A. 2.

REFERENCES

Bowman, J. J. (1967), "High-frequency scattering from an absorbing infinite strip with arbitrary face impedances", Can. J. Phys. 45, 2409-2430.

Felsen, L. B. (1958), "Some aspects of diffraction by variable impedance and anisotropic structures", PIB Electrophysics Group Report No. R-685-58, PIB-613.

Knott, E. F. and T. B. A. Senior (1973), "Non-specular radar cross section study", The University of Michigan Radiation Laboratory Report No. 011764-1-T, AFAL-TR-73-422.

Knott, E. F., V. V. Liepa and T. B. A. Senior (1974), "Non-specular radar cross section study", The University of Michigan Radiation Laboratory Report No. 011062-1-F, AFAL-TR-73-70.

Lamb, H. (1945), Hydrodynamics, Dover, New York, pp. 538-541.

Liepa, V. V., E. F. Knott and T. B. A. Senior (1974), "Scattering from two-dimensional bodies with absorber sheets", The University of Michigan Radiation Laboratory Report No. 011764-2-T, AFAL-TR-

Maliuzhinets, G. D. (1959), "Excitation, reflection and emission of surface waves from a wedge with arbitrary face impedances", Sov. Phys. Doklady 3, 752-755.

Raman, C. V. and K. S. Krishnan (1927), "The diffraction of light by metallic screens", Proc. Roy. Soc. (London), 116A, 254-267.

Senior, T. B. A. (1952), "Diffraction by a semi-infinite metallic sheet", Proc. Roy. Soc., 213A, 436-458.

Senior, T. B. A. (1973), "Tapered impedance half-plane" The University of Michigan Radiation Laboratory Memorandum No. 011764-511-M.